Survivability Investigation of Cylindrical Shaped Water-Cooled Probe in High Heat Flux Conditions

A Thesis Presented for the

Master of Science

Degree

The University of Tennessee, Knoxville

Joshua Osborne

August 2020

Dedication

I would like to dedicate this work to Gregg Beitel who departed during the course of this research. Gregg was an expert at Arnold Engineering Development Complex (AEDC) on cooling probe technology, he designed many of the cooling probes and analytical software used at AEDC, and he developed the COOLWL code that was used in this study. Without Gregg Beitel this work would not have been possible and AEDC would not be as advanced in this challenging technical area.

ACKNOWLEDGEMENTS

First and foremost, I wish to thank my wife Stephanie who has been extremely supportive of me in this process. I would like to thank Dr. Douglas Stefanski for utilizing his expertise in computational fluid dynamics to assist in the understanding of critical heat flux loads and the flow characteristics of particular interest using computational fluid dynamics. I would also like to thank Mr. Devon Parker, who is a leader and a mentor at Arnold Engineering Development Complex, for providing me the resources, motivation, and confidence to complete this work. I'm grateful for my thesis committee members consisting of my major professor Dr. Trevor Moeller, committee member and formerly my professional workplace lead analysis engineer Dr. Milton Davis, and thesis committee member Dr. James Simonton. Lastly, I am thankful to Arnold Air Force Base for providing time and resources to complete this thesis.

ABSTRACT

Diagnostics and data collection downstream of turbine engine augmentors and scramjet combustors provide critical information for turbine engine and scramjet engine developers. One important diagnostic tool is the use of imaging measurement instruments, which are primarily used by the aeropropulsion ground testing community to assess flame holder stability and uniformity in turbine engines. The survivability limitations of these imaging probes are important to understand for use in applications behind ramjet or scramjet engines, where mass flows and exhaust temperatures exceed typical engine augmentor exhaust streams. At a minimum, imaging data acquired behind ramjet and scramjet engines would be used to adjust fuel splits to optimize performance of ramjet and scramjet engines.

The survivability of these metallic imaging probes is due, in part, by an internal water cooling process that is tailored to optimize energy exchange within the metallic structures. A lack of internal cooling would allow temperatures to exceed the melt temperature of the metallic probes, thus resulting in thermostructural failure. At these higher heat fluxes, the cooling flow can transition to nucleate boiling and still remove the required heat away from the metal. When nucleate boiling transitions to film boiling, typically this is referred to as the critical heat flux (CHF). After CHF is the unsteady transition to film boiling which is the situation that occurs where excess vapor blankets inner cooling channel walls, retarding transfer of energy from the heated probe structure to the coolant. For this reason, the prediction of the critical heat flux for expected cooling configurations is necessary to determine survivability and thermostructural margins of safety.

Modeling and simulation efforts to predict critical heat flux in subcooled forced convection flow boiling has made progress, but still leaves a lot to be desired. In particular, an Arnold Engineering Development Complex (AEDC) developed computer code (COOLWL) has been used to analyze nucleate boiling in several backside water cooling configurations. The code includes several

theoretical correlations from literature, in addition to several CHF correlations formulated from experimental data.

This thesis documents work done in the attempt to predict the survivability limits of a cylindrical water cooled device in high enthalpy flows outside the bounds of which the probe has been subjected. Heat flux generated on the outside surface of the probe was predicted using Computational Fluid Dynamics (CFD) with relatively high enthalpy flow conditions and temperatures in excess of 5000 degrees Fahrenheit. Next, the COOLWL code was used to determine if the cooling water was able to avoid reaching critical heat flux while still removing the amount of heat required. The inlet parameters for the COOLWL code were varied including inlet cooling fluid properties and probe insertion depth. A key deliverable from the COOLWL parametric study was to determine the max heat flux conditions the probe could be subjected to before reaching the CHF point. Another key piece of information gained was a realistic convective heat transfer coefficient, in which the process described in this investigation allowed for an analytical way to converge on a realistic value. Lastly, a three dimensional model of the probe was generated and imported into a finite element analysis software (ANSYS) to compute the thermostructural limits, using a realistic heat transfer coefficient gained from the COOLWL analysis. This investigative research delivers a process which systematically acquires two important heat transfer values (critical heat flux and heat transfer coefficient) for thermostructural analysis and survivability of a given backside water cooled configuration. Results of this analysis reduce technical risk and qualifies the cylindrical probe for entry into more extreme temperature and mass flow environments (higher heat fluxes).

TABLE OF CONTENTS

LIST OF TABLES

LIST OF FIGURES

NOMENCLATURE

μ_b	Viscosity of bulk fluid
μ_l	Liquid viscosity
μ_w	Viscosity of fluid at the wall
σ	Surface tension
ρ, ρ_l, ρ_v	Density
v	Kinetic viscosity
AEDC	Arnold Engineering Development Complex
ANSYS	Finite Element Analysis Software
b	Empirical modifier
C	Forced convection constant
$C_{s,f}$	Surface to fluid coefficient (experimentally determined)
CAD	Computer Aided Design
CFD	Computational Fluid Dynamics
CHF	Critical Heat Flux
COOLWL	Cooling fluid to Wall interface critical heat flux correlation code
c_{p_l}	Specific Heat
D	Diameter
D_e	Hydraulic diameter
D_i	Inner diameter divided by π
DoD	Department of Defense
f	Friction factor
FEA	Finite Element Analysis
FORTRAN	Formula Translation programming language
G	Mass flux
g	Gravitational constant
h	Heat transfer coefficient
h_{CHF}	Heat transfer coefficient at CHF point
h_{fg}	Latent heat of vaporization

k	Thermal conductivity
m	Correlation constant
$\frac{L}{D}$, x/d	Length/diameter
n	Correlation constant
N_L	Nusselt Number
p	Pressure
P_r	Reduced pressure (actual pressure divided by critical pressure)
Pr	Prandtl number
q	Heat flux [Btu/ft^2-s]
Q_{avg}	Average heat flux
q_B	Heat flux for full nucleate boiling
q_{Bi}	Heat flux term linear extension of nucleate boiling to incipience
q_c	Heat flux superposition to CHF term
q_{CHF}	Correlation Critical Heat Flux
q_{fc}, $q_{fc_{CHF}}$	Heat flux forced convection term
q_i	Boiling incipience heat flux
Q_{max}	Peak heat flux
q_{pb},$q_{pb_{CHF}}$	Heat flux pool boiling term
q_{tran}	Heat flux transition from boiling incipience to full nucleate boiling
Re	Reynold’s number
ΔT, ΔT_e	Liquid superheat
T	Temperature
T_b	Temperature of bulk fluid
T_w	Surface or wall temperature
$T_{W_{CHF}}$	Temperature of the wall at onset of CHF
T_{sat}	Saturation temperature
T_{sub}	Subcooled temperature
V	Velocity

1.0 INTRODUCTION

1.1 WATER COOLED PROBE SURVIVABILITY

Flow-field characteristic measurements and visual feedback via optical sensors in high-temperature regions of aerospace propulsion systems such as the nozzle exhaust are important to determine many flow-field parameters of interest. These measurements can be obtained at the exit plane or various locations downstream of a combustion system. Typically, the most significant heating environments that exist for these measurement probes are behind augmented turbine engines; however, the potential use in ground testing of ramjet/scramjet propulsion systems dramatically increases the amount mass flow at elevated temperatures, and thus heat flux, these measurement devices would have to endure. Survivability of internally forced convection water cooled probes in these applications that aren't commonly visited becomes a challenge.

Increased survivability is largely due to an internal cooling water process tailored to optimize energy exchange within metallic structures. Without internal cooling, these probe temperatures would exceed the melting point of almost all existing materials. Even with use of internal cooling water techniques there are still boiling limits of the cooling fluid, and these limits are specific to the configurations of the probes.

The investigation reported herein was to determine analytically if an existing probe geometry would be able to survive high enthalpy flows, and at what approximate heat flux the probe would fail. To help mitigate cost of possible failures, it is important to understand current measurement probe design limits as heat loads that they are needed to endure increase. This understanding enabled parametric variations of cooling water characteristics to the current probe design. Parametric variations allowed for an analytical method to be applied for predicting and understanding of the critical heat flux (CHF), and thus allowed for thermal performance optimizations.

1.2 CRITICAL HEAT FLUX CORRELATIONS

Understanding of CHF is vital to ensure the survivability of water cooled probes in high heat flux environments. CHF is the point at which heat transfer between a heated wall and cooling fluid starts to decrease because cooling fluid is transitioning to more of a vapor concentration than that of a liquid. This transition to vapor often leads to material failure as the local surface temperature rises in the area where vapor starts to form, and this surface temperature rise is due to the vapor's lower thermal conductivity. This transition to vapor in localized areas is commonly referred to as film boiling [1]. A simplified schematic shown in Figure 1 displays the flow of a fluid as it transitions from a single-phase liquid to a point just before and after CHF.

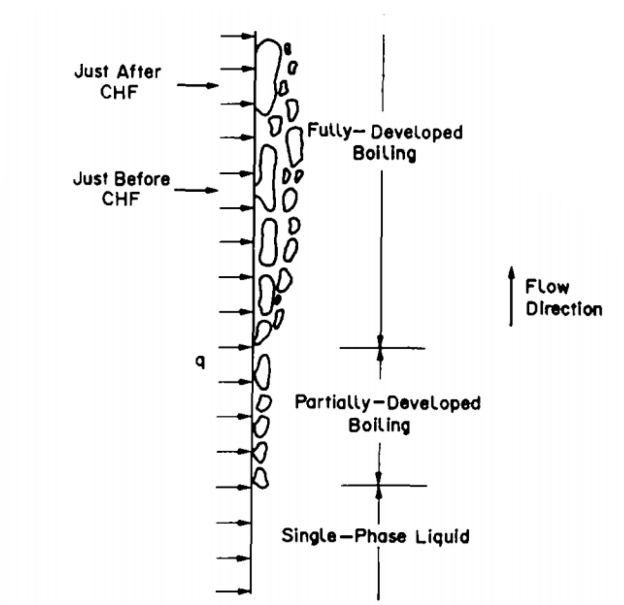

Figure 1. Flow Transition from Single-Phase to CHF [1]

To date, there are thousands of empirical and semi-empirical CHF correlations used by design engineers on applications dealing with high heat flux environments. Unfortunately, most correlations have been developed for particular configurations using limited data sets. In order to successfully predict and optimize thermal performance of an existing hardware design, it is necessary to understand which correlations are applicable to the configuration of interest. This research includes investigation and justifications into multiple CHF correlations used to perform analysis and optimize thermal performance of given use cases defined herein.

The investigations in this study focused on keeping the system below predicted CHF values and in the nucleate boiling regime. Evaluating and optimizing thermal performance effects of cooling parameters on the periscope probe system of interest could possibly led to use of the hardware in more extreme heat flux environments of interest. Collecting data via the periscope probe in such extreme environments, would provide invaluable information to AEDC and other industries needing high enthalpy flow diagnostic data.

2.0 LITERATURE REVIEW

To enable application of predictive nucleate boiling and CHF correlations on a unique cooling probe system, a review was completed of boiling characteristics and variable parameters that affect boiling behaviors. A more extensive review on the many parameters which can affect cooling performance in various applications can be found in Bietel [2]. Beitel reported on research, completed over the period of three years, that was a compilation of several other's work performed since the 1950s. Beitel's high level summaries and extensive list of 391 references provided a very useful starting point and guide for this literature review.

2.1 CHARACTERISTICS OF THE BOILING CURVE

The boiling curve was first introduced by Nukiyama [3] in the 1930s and was used to present a system's temperature response as heat flux is increased on a surface cooled by an adjacent fluid. This figure of merit has since been commonly used to describe the different phases that cooling liquids go through as the fluids increase beyond saturation temperature. Figure 2 shows the typical shape of a boiling curve, obtained when heat flux (q) from a cooled surface is plotted as a function of the liquid superheat (ΔT), in which liquid superheat is defined by the difference between surface or wall temperature (T_w) and liquid saturation temperature of the cooling fluid (T_{sat}).

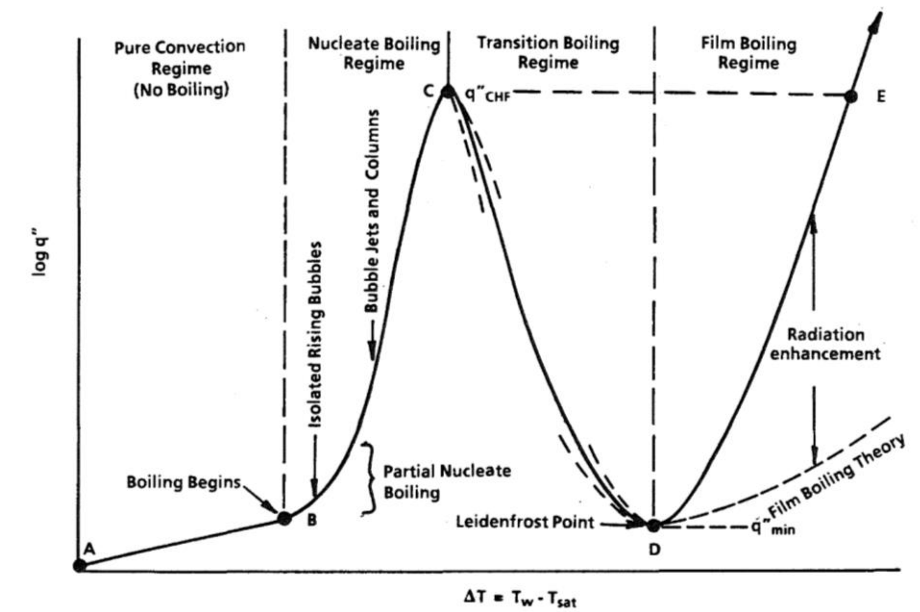

Figure 2. The Basic Boiling Curve [2]

The pure convection regime in Figure 2 is the result of the surface temperature remaining below the saturation temperature of the cooling fluid. Cooling at low heat flux is by pure convection heat transfer and is well understood. In this region, analytical solutions and experimental correlations allow for accurate prediction of heat transfer in various cooling configurations [2].

The nucleate boiling regime in Figure 2 occurs when wall surface temperature becomes significantly greater than water saturation temperature. This causes boiling to occur from discrete nucleation sites (vapor bubbles form) on the surface. Just to the right of point B in Figure 2, bubbles tend to burst on or near the surface allowing subcooled liquid to reattach to the wall. As you move further away from point B and start to get closer to the CHF (point C), then bubble columns start to form and move into the bulk fluid. This regime is most desired from a thermal performance perspective as bubbles are rapidly moving heat away from the wall and into the bulk fluid, and conversely allowing the bulk fluid to reattach to the surface wall.

An example of these bubbles forming and traveling into bulk fluid during nucleate boiling can be seen in Figure 3. As critical heat flux is approached on the curve of Figure 2, an unstable transition to film boiling begins. During CHF, phase change causes vapor bubbles to begin combining near the surface and this can be seen by the example in Figure 4. While the CHF point is ideal for optimal thermal performance, the goal is to never reach it because of unstable film boiling that can occur just past or around the CHF. To the right of the CHF point on the curve in Figure 2 is where film boiling starts to occur and this is illustrated by the example in Figure 5. During film boiling, vapor effectively insulates the surface from effective heat transfer to the liquid. As previously mentioned, when a cooling system goes past the CHF point, boiling becomes highly unstable and thermostructural failure is inevitable.

Figure 3: Nucleate Boiling Illustration [4]

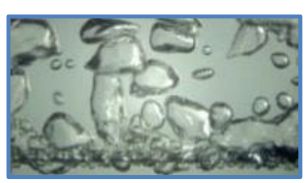

Figure 4: Critical Heat Flux Illustration [4]

Figure 5. Film Boiling Illustration [4]

2.2 PARAMETRIC VARIABLES AND THE EFFECTS ON CHF

Many variables affect the cooling process and CHF values. Beitel [2] documented that some parameter effects are prevalent all the way along the boiling curve, while others are more dominant in certain areas of the curve. Also, parameter to parameter interactions exist where changes in one parameter affect another parameter, but this study does not quantify those interactions specifically. More so, the contribution of each individual parameter on CHF limit was the primary interest in understanding parameter effects on the boiling curve. Furthermore, parameters that are physically possible to vary with direct implications in this investigation were of more concentration. For example, the cooling water pressure can be easily altered in this application for testing, while parameters like material type the probe is constructed of is more of a fixed variable. The literature review in this section was used to gain knowledge for predictions and for the attempts to optimize thermal performance backside water cooling on the cylindrical water cooled probe.

2.2.1 COOLING FLUID PARAMETERS

The most applicable parameters that were varied in this study deal with the bulk cooling fluid. Mass flux, subcooling, pressure, coolant type, turbulence, and flow instabilities are major properties of cooling fluids that have effects on critical heat flux. Mass flux, subcooling, and pressure are parameters that have direct implications to the scope of this study and can be easily altered without major hardware design changes.

Mass flux at which water is traveling through a cooling passage has a significant effect on CHF. Mass flux, or flow velocity, is what enables the forced convective boiling heat transfer that occurs when the bulk fluid is in motion. If the boiling fluid is not flowing, then it is simply referred to as saturated pool boiling. The thermal advantages of the forced convection are not obvious until boiling occurs. McAdams demonstrated through experiments that CHF could be increased by increasing fluid mass flux [5]. Figure 6 suggests higher CHF values and burnout points can be reached as mass flux, or fluid velocity, is increased.

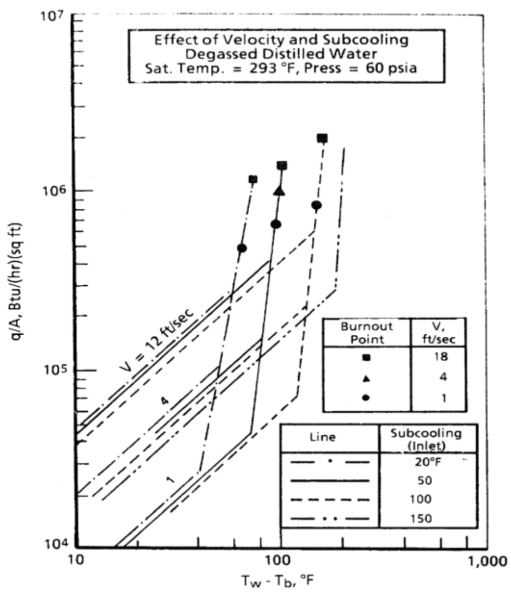

Figure 6. Effect of Velocity and Subcooling [5]

Mattson et al. [6] also proved that velocity can affect CHF by the diminishing and decreasing of bubble quantity and size at higher velocities. Another important discover they observed was the macroscopic view of the fluid as it reached CHF. They reported there was no sudden change to two-phase flow in the bulk fluid, and instead it was a thin continuous vapor layer along the heated surface.

Subcooling is defined as the difference in fluid bulk temperature below fluid saturation temperature. Subcooling, like velocity, has a similar effect on the boiling crisis in that its primary advantages exist up until the CHF is reached. McAdams [5] showed, in Figure 6, that subcooling has some effect on heat transfer in the pure convection region; however, it was Huff and Rousar [as cited in Beitel 2] that discovered subcooling along with velocity are the two most important variables on

CHF. The work of Huff and Rousar concluded, with combining velocity and an average subcooling temperature, to derive a linear fit to supporting experimental data. This correlation is still compared to applications today, and was helpful in illustrating CHF increases with an increase in subcooling.

Pressure is directly related to the saturation temperature of cooled fluids; therefore, it plays a key role in the operating location on the boiling curve. It has been found that increasing pressure will benefit the CHF up to a certain point. Cichellie and Bonilla [7], studied various cooling fluids in a pool boiling experiment and discovered that increasing pressure will increase the CHF up until about one third the critical pressure of the fluid. The critical point of water is at approximately 705 degrees Fahrenheit and 3,200 psia, and they found that the benefits of raising CHF was negligible after approximately 1000 psig. Addoms [8] also performed a pool boiling experiment that yielded similar results. Mishima et al. [9] was able to trend CHF as a function of pressure and mass velocity for an internally heated annuli, and these trends matched well with the Katto [10] correlation. Boyd [11] made the same conclusions that optimum pressures existed as functions of mass flow, as seen in Figure 7.

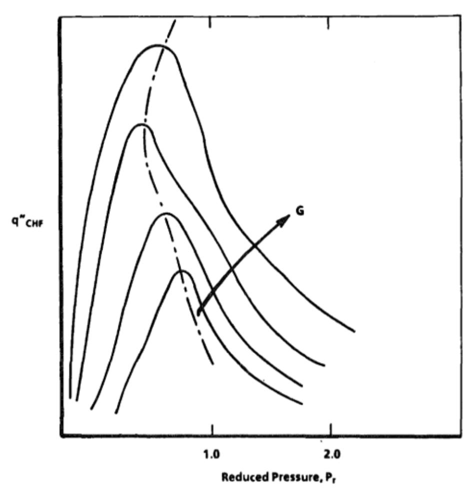

Figure 7. Optimum Pressure as a Function of Mass Flux [11]

Coolant type, turbulence, and flow instability effects on CHF will not be a variable and main parameter of interest in this research and will not be considered for parametric variations. However, recommendations into the design will be considered from a holistic sense using knowledge gained from the detailed parameter contribution compiling of Beitel [2].

2.2.2 MECHANICAL PARAMETERS

The effects of mechanical parameters on CHF were considered and include surface roughness, wall material, wall thickness, geometry, aging, deposits, and coatings. All of these mechanical parameters will not be able to be parametrically varied going forward in this research, but some specific attention is given to a few of the mechanical fixed variables to aid in the understanding of the methodology on the application in this study, and will aid in recommendations for designs enhancements for future cooling probe designs.

Surface roughness is found by several scientists to have an effect on CHF, some more so than others. Jabardo [12] performed an experiment with refrigerants R-123 and R134a in copper and brass tubes that verified many surface roughness arguments in previous experiments. Jabardo proved the general trends in surface roughness, reported on by Corty and Foust [13], Kozitskii [14], Nishikawa et al.[15], and others. These general trends show an increase in CHF with increasing surface roughness. However, Bergles and Morton [16], Leung et al [17], and O'Hanely et al. [18] investigated surface roughness and could not find any discernable correlation between surface roughness and CHF. O'Hanely et al. found CHF effects from surface porosity could potentially enhance CHF up to 60% with hydrophilic pores (water pulled to the surface), and decrease CHF up to 97% with hydrophobic pores (surface repels water).

Wall material effects on CHF was first demonstrated by Rohsenow [19] in his nucleate boiling correlation. Table 1 shows values of surface to fluid coefficients and exponents for Rohsenow's equation of various surface to fluid combinations, and this is discussed further in the following Section 2.3. Vachon et al. [20] went on to apply the Rohsenow equation to eleven literature data sets and concluded that the liquid to surface combinations indeed had an effect.

Table 1. Values of $C_{s,f}$ for Various Surface-Fluid Combinations [21]

Surface–Fluid Combination	$C_{s,f}$	n
Water–copper		
Scored	0.0068	1.0
Polished	0.0128	1.0
Water–stainless steel		
Chemically etched	0.0133	1.0
Mechanically polished	0.0132	1.0
Ground and polished	0.0080	1.0
Water–brass	0.0060	1.0
Water–nickel	0.006	1.0
Water–platinum	0.0130	1.0
n-Pentane–copper		
Polished	0.0154	1.7
Lapped	0.0049	1.7
Benzene–chromium	0.0101	1.7
Ethyl alcohol–chromium	0.0027	1.7

Wall thickness has a relatively small influence on CHF compared to some of the other major parameters. Delvallem and Kenning [22] showed that thin walls ranging from 0.08-0.2mm in thickness had increased heat transfer with increasing wall thickness, and this can be seen in Figure 8. However, flow orientation is more of an influence than the wall thickness. Winovich and Carlson [23] showed that CHF increased by as much as 100% going from 3mm to a thinner width of just 2mm; however, it is likely because of the use of undulating concave flow surfaces.

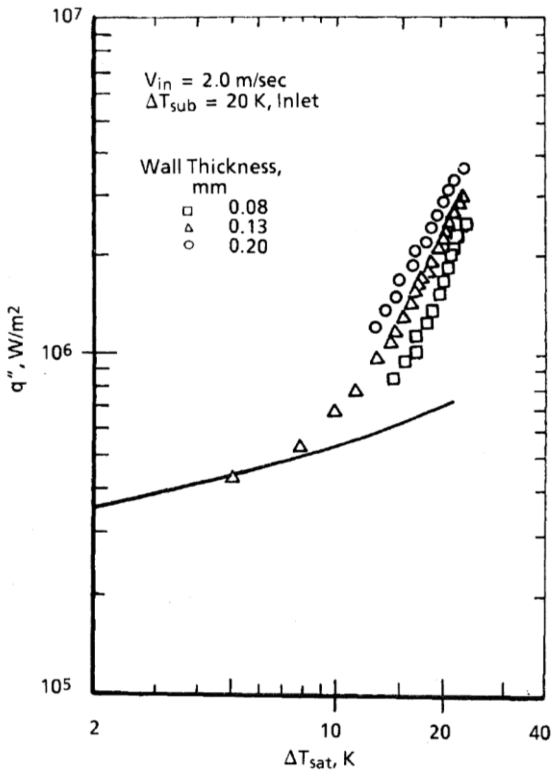

Figure 8. Influence of Wall Thickness on Boiling

Geometry of cooling passages has been shown to affect the heat transfer of the cooling fluid to the wall surface. While parameters such as length are intuitive because it increases the amount of heat flux the cooling fluid needs to remove, other things such as the channel diameter and cross section shape are more difficult to discern. Katto [24] developed a CHF model using validation data, and discovered an interesting fact, that CHF conditions vary with a change in tube diameter. One year later Katto [25] experimentally proved that theory and showed decreasing diameter increases CHF on six different types of fluids (water, R-12, R-11, nitrogen, helium, and R-113). Bergles [26] also completed experiments, displayed in Figure 9, that showed CHF limits increases with a decrease in diameter. Concave, convex, and straight cooling passages were studied by Hughes [27] who found that CHF was increased by up to 50% for concave cooling passages compared to straight sections, and conversely, he discovered convex sections to be approximately 22% lower compared to the straight section.

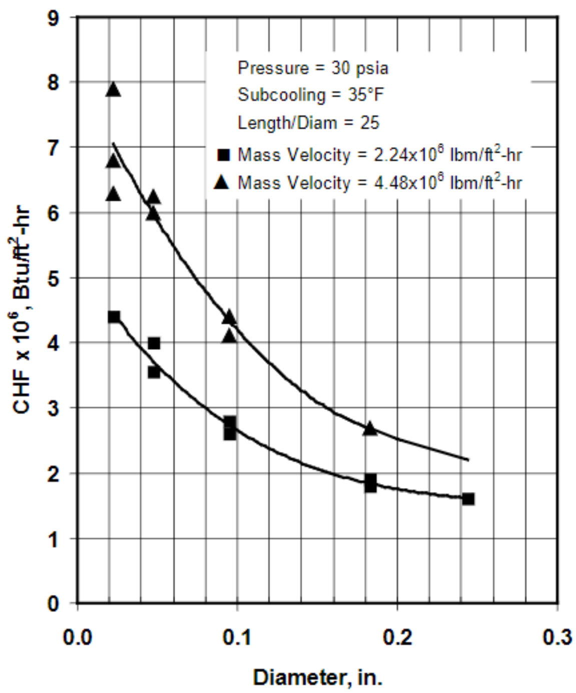

Figure 9. Effect of Tube Diameter on CHF [26]

2.3 HEAT TRANSFER PRIOR TO BOILING

There are a few variations of turbulent flow heat transfer correlations, with some developed as early as the 1930s. These correlations focus on determining expressions for Nusselt number, which is a dimensionless ratio of convective to conductive thermal resistance of a fluid to surface thermal boundary layer. This section will discuss five variations of the basic single phase forced convection heat transfer expression shown in Equation 1 [21]. Where 'N_L' stands for the local Nusselt number, 'C' is an applied forced convection constant that varies between correlations, ‘Re’ is the local Reynolds number (a dimensionless term that specifies flow as laminar or turbulent), ‘m’ and ‘n’ are constants that vary between correlations, and ‘Pr’ is the local Prandtl number (which is a dimensionless term that compares thickness of fluid momentum and thermal boundary layer).

$$N_L = CRe_L^m Pr^n \tag{1}$$

This Nusselt number and Reynolds number relationship was first used by Dittus and Boelter [21] for turbulent flow, and is shown in Equation 2.

$$N_L = 0.0265 Re_L^{0.8} Pr^{0.4} \tag{2}$$

Colburn then went on to adjust the coefficients for heat transfer inside tubes, and this is shown in Equation 3. [28]

$$N_L = 0.023 Re_L^{0.8} Pr^{1/3} \tag{3}$$

Sieder and Tate discovered that because fluid properties changed significantly as a function of temperature, corrections were needed to compensate for changing fluid properties, specifically viscosity [28]. This expression is shown in Equation (4), where ‘μ_b’ is viscosity of bulk fluid temperature, and ‘μ_w’ is the viscosity of the fluid at the wall temperature.

$$N_L = 0.027 Re_L^{0.8} Pr^{1/3} \left({}^{\mu_b}/_{\mu_w}\right)^{0.14} \tag{4}$$

Carpenter et al. [29] with the help of Colburn, then modified the equation for use with annuli, as seen in Equation (5). Coincidently, the ‘C’ constant was changed back to the ‘0.023’ value that Coburn had originally formulated; however, the equation is still more complex than what Coburn had originally conceived.

$$N_L = 0.023 Re_L^{0.8} Pr^{1/3} \left({}^{\mu_b}/_{\mu_w}\right)^{0.14} \quad (5)$$

Petukhov [30] went on to improve the accuracy of the mathematical model and his work has been evaluated and concluded by many other researchers in literature to be much more accurate than the above mentioned correlations (Equations 2-5). Petukhov has a very complex set of calculations that yield high accuracy but are not shown herein, nevertheless his simplified version of those calculations can be condensed into one version shown in Equation 6.

$$N_L = \frac{Re\,\mathrm{Pr}\,\left(\frac{f}{8}\right)}{1.07 + 12.7\left(Pr^{2/3} - 1\right)\sqrt{{}^{f}/_{8}}} \quad (6)$$

Where ‘f’ is a friction factor valid between $10^4 \leq Re \leq 5 \times 10^6$ (turbulent) for smooth pipes. Equation 7 can be used to calculate ‘f’. Other values for ‘f’ can be acquired from the Moody chart for smooth and rough pipes. [2]

$$f = (1.82 \log Re - 1.64)^{-2} \quad (7)$$

While Sleicher and Rouse [28] went on to complement Petukov’s equation with an attempt at an even more simplified version, the formulation is not shown herein and not used in the analytical tools of this investigation as it is viewed as redundant by the author.

Using the Nusselt number approximations, heat transfer coefficients can be computed in Equation 8. ‘h’ is the resulting non-boiling heat transfer coefficient, ‘k’ is thermal conductivity of the fluid, and ‘D’ is the inside diameter of the cooling passage.

$$h = \frac{N_L k}{D} \tag{8}$$

The heat transfer coefficient can then be applied to Newton’s law of cooling, which yields the forced convective heat flux equation shown in Equation 9. Where ‘q_{fc}’ is the forced convection heat flux up to the inception of boiling point, ‘Δt_{sat}’ is the temperature difference between the wall temperature and saturation temperature of the fluid, and ‘Δt_{sub}’ is the temperature difference between the fluid saturation temperature and the bulk fluid temperature.

$$q_{fc} = h\,(\Delta t_{sat} + \Delta t_{sub}) \tag{9}$$

2.4 TRANSITION TO BOILING

There are many correlations that try to predict the inception of flow boiling, and the point at which flow boiling becomes completely nucleate boiling. Figure 10 shows an area where boiling begins, which is often referred to as incipient boiling, and also draws attention to the area of partial nucleate boiling. The area highlighted on the curve in Figure 10, between partial nucleate boiling and CHF, indicates that the fluid has transitioned to full or complete nucleate boiling, and is often referred to as flow boiling.

Many researchers have presented work in this transition region from single phase forced convection to flow boiling. Bergles and Rohsenow [31] compared the results of some of the common estimations used from McAdams et al. [32], Kutateladze [33], Rohsenow [19], and Forster and Greif [34], and this comparison can be seen in Figure 11.

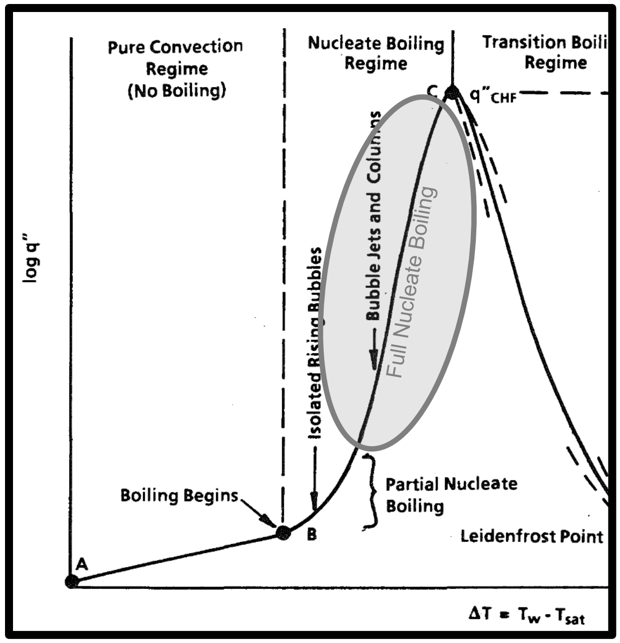

Figure 10. Boiling Curve Focused on Nucleate Boiling [2]

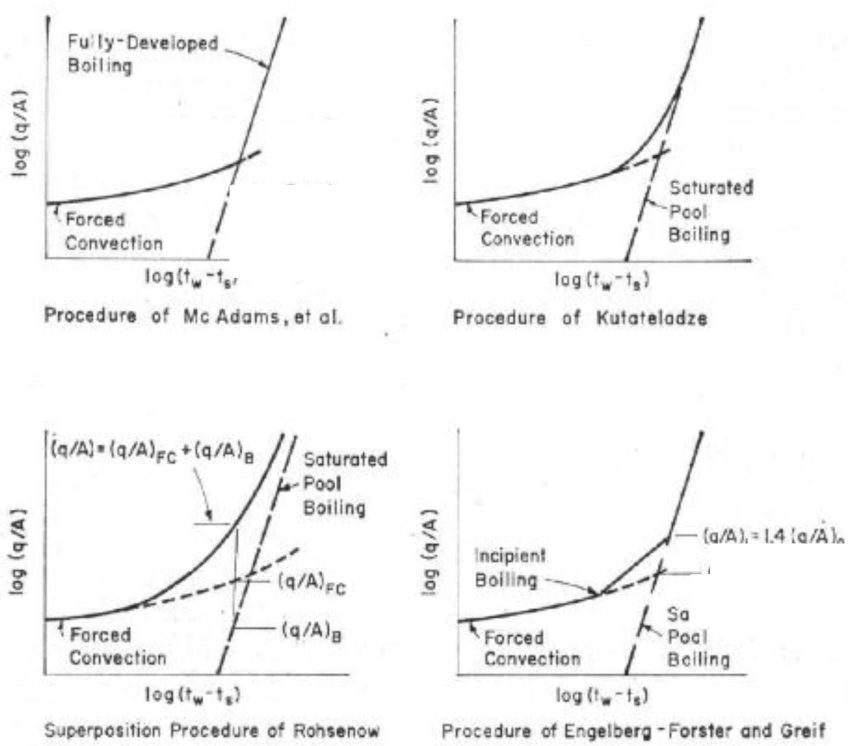

Figure 11. Comparison of Forced Convection Transition to Flow Boiling [31]

McAdams et al. [32] were the first to apply an empirical correlation for this transition region. Kutateladze [33] and Forster and Greif [34] generated empirical correlations using pure forced convection calculations and heat flux results from pool boiling. As suggested by the word ‘pool’, pool boiling is the boiling of a liquid in low velocity or stagnate flow, and is not referring to the forced convection boiling discussed in this research. Bergles and Rohsenow [31] went on to show that using experimental heat fluxes from saturated pool boiling is not completely accurate, as seen in the lower left hand corner of Figure 11. However, it was Rohsenow [19] himself that first developed the commonly used and iterated upon relationship seen in Equation 10. Here, ‘q_{tran}’ is the heat flux during transition from forced convection to full nucleate boiling, ‘q_{fc}’ is the forced convection heat flux, and ‘q_{pb}’ is a correlated (by superposition) pool boiling heat flux term.

$$q_{tran} = q_{fc} + q_{pb} \tag{10}$$

Where

$$q_{pb} = \mu_l h_{fg} \left[\frac{g(\rho_l - \rho_v)}{\sigma}\right]^{1/2} \left(\frac{c_{p,l}\Delta T_e}{C_{s,f} h_{fg} Pr_l^n}\right)^3 \tag{10a}$$

Here, ‘μ_l’ is the liquid viscosity, ‘h_{fg}’ is the latent heat of vaporization, ‘$C_{p,l}$’ is the specific heat of the liquid, ‘ΔT_e’ is the liquid superheat, ‘$C_{s,f}$’ is the surface fluid combination obtained from Table 1, ‘g’ is the gravitational constant, ‘ρ’ is the density of the liquid and vapor, 'σ’ is the surface tension, and ‘n’ is a dimensionless exponent obtained from Table 1.

As previously mentioned, Bergles and Rohsenow [31] more accurately determined the correlation by correcting the ‘q_{bp}’ term to include nucleate boiling relationships instead of saturated pool boiling. Their correlation for the transition region can be seen in Equation (11). Where 'q_B' is the calculated term for the fully transitioned nucleate boiling region, and 'q_{Bi}' is the term that is a linear extension from the fully developed nucleate boiling region.

$$q_{tran} = q_{fc}\sqrt{1 + \left\{\frac{q_B}{q_{fc}}\left(1 - \frac{q_{Bi}}{q_B}\right)\right\}^2} \tag{11}$$

A simplified version of the q_{Bi} term (q_i) was then determined by Bergles and Rohsenow shown in Equation 12. They formulated this term, which is accurate for a pressure range of 15-2,000 psia, by predicting the onset of bubble nuclei from combining the Helmholtz relation and the Clapeyron equation [31]. Where 'q_i' is prediction at boiling incipience and 'p' is the pressure.

$$q_i = 15.60p^{1.156}(T_W - T_{sat})^{2.3/p^{0.0234}} \tag{12}$$

This resulting transition from forced convection to nucleate boiling correlation and the recently described correlations are best viewed on a boiling curve in Figure 12.

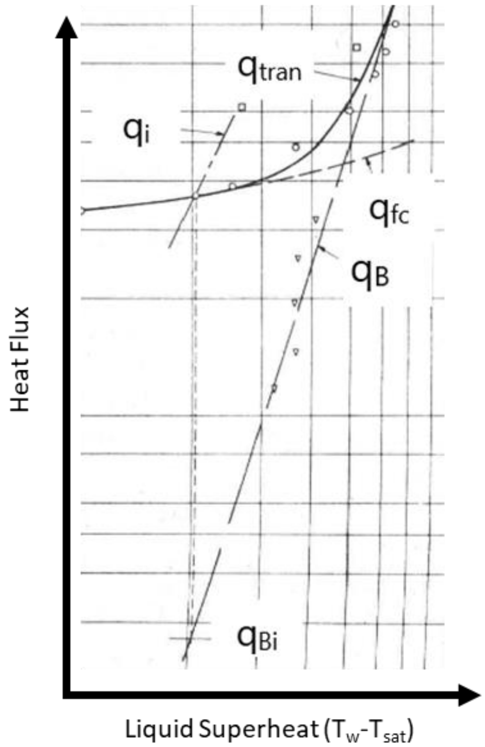

Figure 12. Nucleate Boiling Heat Flux Correlation Terms [31]

2.5 PREDICTIVE CHF CORRELATIONS

As previously discussed in Section 2.2, many parameters have influences on CHF values. The variety of parameter effects are not completely different compared to the nucleate boiling region of the boiling curve; however, the complexity and unsteady nature give a wider range of variation between correlations. The CHF correlations discussed in this section are both semi-empirical and empirical. There is no CHF correlation that exists to cover all the possibilities for use in every backside water cooling configuration and use case. As such, these correlations require a knowledge of various parameters used and wide range of test conditions which make up the data sets these models were validated and fitted against.

2.5.1 SEMI-EMPIRICAL BASED CHF CORRELATIONS

Gambill [35] developed a semi-empirical model which used the Rohsenow's nucleate flow equation from Equation 10 and extended it to predict CHF shown in Equation 13. Where 'q_{CHF}' is the predicted CHF, '$q_{fc_{CHF}}$' is a modified force convection heat flux term, and '$q_{pb_{CHF}}$' is the nucleate boiling heat flux term modified to extend to CHF.

$$q_{CHF} = q_{fc_{CHF}} + q_{pb_{CHF}} \tag{13}$$

$q_{pb_{CHF}}$ is defined in Equation 14 [35]. Here units for the parameters are as follows: $q_{pb_{CHF}}$ is in $\frac{BTU}{ft^2hr}$, 'D_e' is the hydraulic diameter of the cooling passage in ft, 'D_i' is the diameter of the heated surface in ft, and 'V' is the velocity in ft/s. Also note these values are for 'D_e' < 0.1 ft, which is in the range of interest for this research.

$$q_{pb_{CHF}} = 1.8\left[10890\left\{\frac{D_e}{D_e+D_i}\right\} + \frac{48}{{D_e}^{0.6}}V\right](T_W - T_b) \tag{14}$$

The hydraulic diameter is defined in Equation 15. Here, 'A' is the cross sectional area of the flow, and 'P' is the perimeter.

$$D_e = \frac{4A}{P} \tag{15}$$

The wall temperature 'T_W' is determined using Bernath [37] wall temperatures at different measured burnout conditions of pressure, 'P', and velocity, 'V'. Gambill found that these correlations matched well for water, and in most cases was within 20% of the test data compared against. This simplified version of 'T_W' is shown in Equation 16.

$$T_w = 57lnP - 54\left(\frac{P}{P+15}\right) - \frac{V}{4} \quad (16)$$

Levy [38] proposed a similar approach using superposition, and included an additional term 'q_c' seen in Equation 17. Also, several terms are added for liquid and vapor which include thermal conductivity of liquid 'k_l', density of liquid 'ρ_l' and vapor 'ρ_v', heat of vaporization 'h_{fg}', surface tension 'σ', gravitational constant 'g', and q_{fc} can be obtained from Equation 9.

$$q_{CHF} = q_{fc} + q_{pb} + q_c \quad (17)$$

Where

$$q_{pb} = 0.131 h_{fg}\rho_v \left[\frac{\sigma g^2(\rho_l - \rho_v)}{\rho_v^2}\right]^{1/4} \quad (18)$$

And

$$q_c = 0.696\sqrt{k_l \rho_l c_{p_l}} \left[\frac{(\rho_l - \rho_v)}{\sigma}\right]^{1/4} \left[\frac{\sigma g^2(\rho_l - \rho_v)}{\rho_v^2}\right]^{1/8} \Delta T_{sub} \quad (19)$$

2.5.2 EMPIRICAL CHF CORRELATIONS

Bernath [37] extended his earlier work to include various geometries, and it is described in the following set of equations. 'h_{CHF}' is in $\frac{BTU}{ft^2 hr\,°C}$, '$T_{W_{CHF}}$' is the wall temperature at CHF in degrees Centigrade, 'T_b' is bulk fluid temperature and is also in degrees Centigrade, 'V' is velocity in $\frac{ft}{sec}$, 'D_i' is the inner diameter (in ft) divided by π, and 'D_e' is the hydraulic diameter of the cooling passage in ft. Also note these values are for 'D_e' < 0.1 ft, which is in the range of interest for this research.

$$q_{CHF} = h_{CHF}\,(T_{W_{CHF}} + T_b) \tag{20}$$

Where $T_{W_{CHF}}$ is the same as T_W in above in Equation 16.

And

$$h_{CHF} = 19{,}602\left[\frac{D_e}{D_e+D_i}\right] + \left(\frac{86.4}{{D_e}^{0.6}}V\right) \tag{21}$$

This Bernath correlation is one of the most reliable and more accurate (+/-16%) prediction calculations that exist in the parameter ranges of interest. The ranges include high pressure up to 3,000 psia, velocity from 4 to 54 ft/sec, subcooling from 0 to 615 degrees Fahrenheit, and hydraulic diameters from 0.143 to 0.66 inches.

Van Huff and Rousar [as cited in Beitel 2] developed correlations with 23 different fluids up to 2,000 psia, velocities of 7.5 to 205 ft/sec, and bulk cooling temperatures of 76˚F to 470˚F. This expression is shown in Equation 22.

$$q_{CHF} = 5.1 + 0.000860V\Delta T_{sub} \tag{22}$$

Labuntsov [39] experimentally developed and fitted Equation 23 to test data on areas of interest up to close to 2,900 psia. Here, ‘k’ is thermal conductivity, ‘v’ kinetic viscosity, ‘ρ’ is density, and ‘b’ is an empirical multiplier that depends upon pressure.

$$h_{CHF} = q_{CHF}^{2/3}b\left[\frac{k^2}{\sigma v_l T_{sat}}\right]^{1/3} \tag{23}$$

Where

$$b = 0.075\left[1 + 10\frac{\rho_v}{\rho_l - \rho_v}\right]^{2/3} \tag{24}$$

Vandervort, et al. [40] developed a 5 parameter correlation which accounts for changes in mass flux, bulk fluid temperature, pressure, cooling passage diameter, and length to diameter ratio. These 5 terms are described in the CHF correlation shown here in Equations 25-30, where 'G' is the mass velocity.

$$\begin{aligned} q_{CHF} = {} & 17.05\left[(G')^{0.0732+0.239\,D'}\right] \\ x & \left[(T')^{0.3060G'+0.00173T'-0.239\,D'}\right] \\ x & \left[(P')^{-0.1289}\right] \\ x & \left[1 + (D')^{-2.946+0.7821G'-0.009299\,T'}\right] \\ x & \left[1.540 - 1.280\left(\frac{L}{D\prime}\right)\right] \end{aligned} \tag{25}$$

Where

$$G' = 0.005 + \frac{G}{10^5} \tag{26}$$

$$T' = 5 + \Delta T_{sub} \tag{27}$$

$$P' = \frac{(0.0333+p)}{3} \tag{28}$$

$$D' = \frac{D}{0.003} \tag{29}$$

$$\frac{L}{D\prime} = \frac{L}{D}\Big/40 \tag{30}$$

The units for the above equations are as follows: ‘G’ in $\frac{kg}{m^2 sec}$, ‘ΔT_{sub}’ in degrees Centigrade, ‘p’ in MPa, ‘D’ in meters. This Vandervort correlation historically correlates within approximately 25% over the ranges of interest for this study, except for $\frac{L}{D}$, which this investigation requires more than double the correlation range.

2.6 CONCLUSIONS FROM LITERATURE REVIEW

CHF empirical correlations are the most accurate to an application, if the driving control parameters of interest are close in value. However, not many correlations exist across the regime where high heat flux micro-channel cooling environments will be subjected to the correct combination range of high fluid pressure, velocity, subcooling, small cooling channel diameter and fluid type. In most correlations high errors exist when comparing the models to test data in which it is calibrated and, in some cases, require extrapolation outside of available data. Extrapolation in this sense is not ideal, and in all cases semi-empirical correlations should be used to assess the range of values provided by empirical correlation predictions to make sure solutions follow the general trends of physics.

Uncertainty from a measurement uncertainty standpoint is also another area of concern. There has been a lack of reporting on data measurement uncertainty for all of the test data that has been used to generate these empirical based CHF prediction models. Obviously, this means that extreme caution should be taken when using these CHF correlations for new designs or for understanding existing hardware like this investigative approach described herein.

Aside from all of the unknown uncertainties associated with applying CHF correlations to a unique application, there are known uncertainties reported on for the correlations applied to the test data used for validation. Also, others have reported on large uncertainties of plus or minus 100 percent when using the Roshenow nucleate boiling correlations.

2.7 PROBLEM STATEMENT

The goal of this investigation was to assess and select appropriate correlations to predict the CHF of a cylindrical water cooled imaging probe of fixed geometry in high heat flux environments. Water inlet parameters were varied in the CHF formulations, within practical limits possible for the application, in order to optimize thermal performance and survivability. Maximum predicted CHF values for the configuration were predicted. The correlations determined relevant heat transfer coefficient values used in a thermostructural analysis. Heat transfer coefficient values were determined by summing the heat transfer coefficients gained from forced convection and nucleate boiling. The nucleate boiling heat transfer coefficient was determined using the Rohsenow pool boiling heat flux value gained from Equation 10a.

3.0 BACKGROUND

3.1 COOLWL

COOLWL is a FORTRAN based computer code developed by AEDC to improve understanding of the heat transfer processes and subcooled forced convection nucleate boiling. The code performs a steady-state energy balance across a surface fluid interface given an input heat flux, wall material, geometric configuration, fluid properties, and flow conditions. These calculations enable the computing of surface temperatures, heat transfer coefficients, and critical heat flux values.

Several forced convection and nucleate boiling models, including Rohsenow [47], are provided in the code. COOLWL does not include any theoretical models for predicting CHF, because such theoretical models show basic trends from parameter effects at best. Yuan et al [48]. recently did extensive work in generating a CHF predictive model, but the results are supportive that only general trends can be predicted. There are over 50 empirical correlations from literature incorporated into the COOLWL code, but only a few are applicable to scope of this research which deal with small diameter annular flow configurations, commonly referred to as micro-channels. However, because Katto [24] and Bergles [26] showed increasing cooling tube diameters reduced CHF, some larger diameter annular flow correlations, such as Van Huff and Rousar [as cited in Beitel 2] and Labuntsov [39], were assessed. These slightly larger diameters were used in comparison to smaller micro channel applications and this provided a conservative CHF comparison.

A small subset from a large list of CHF correlations available in the COOLWL code were chosen to aid in this investigation. They are discussed in more detail in Section 2.5, and are as follows:

- Bernath [37] (main correlation used, most conservative)
    - Good correlation for water (historically +/- 20%)
    - Parameters within range of interest are: pressure, velocity, heat flux, tube diameter, and subcooling temperatures
- Levy [38]
    - Predictions up to 2,000 psia water usually within +/- 30%
- Vandervort, et al. [40]
    - Results general accurate to +/-25%
    - Extrapolations will exist for length to diameter ratio and pressure to capture ranges needed in this investigation
- Van Huff and Rousar [as cited in Beitel 2] and Labuntsov [39].
    - All parameters in range of interest except diameters are at 2-4 times bigger, which as previously stated can provide a conservative answer
- Rohsenow [19] nucleate boiling correlation
    - Used to establish a point of reference on the boiling curve

3.2 CYCLINDRICAL PERISCOPE PROBE

3.2.1 PERISCOPE PROBE INTRODUCTION

The AEDC developed periscope-style imaging probe, shown in Figure 13, is routinely used behind turbine engine exhausts during augmentor operations. Figure 14 shows the periscope probe in operation behind an augmentor exhaust stream. Exhaust temperatures these probes endure are in excess of 3,500˚F [42], and some probes have been in operation over a decade without failure. Survivability of these probes is mostly due to the robust cooling design that takes advantage of high pressure water in several small cooling passages to remove the heat from the wall. Inside passages and inner core of the probe are constructed of press-fit stainless steel, while the outer shell is an electroformed nickel. Earlier versions of this design used a stainless steel outer shell, but the design was changed to electroformed nickel to take advantage of not only more complex shapes that are enabled by the electroforming technique, but also advantages gained by an optimized fluid to surface combination (water and nickel). Advantages gained from the fluid to surface combination were described from the nucleate boiling correlation developed by Rohsenow [19]. A cutaway view of the structure can be seen in Figure 15, while Figure 16 shows the imaging data collected from looking into a turbine engine augmentor.

Figure 13. Imaging Probe [42]

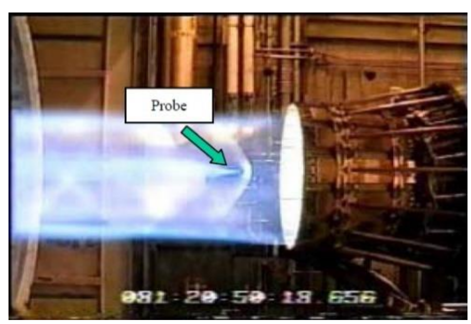

Figure 14. Probe in Operation [42]

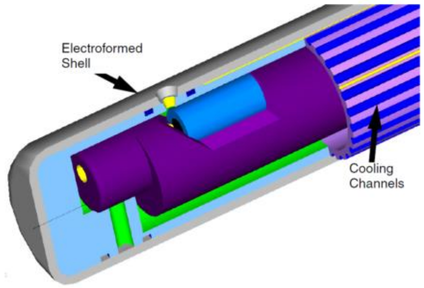

Figure 15. Cutaway of Probe [43]

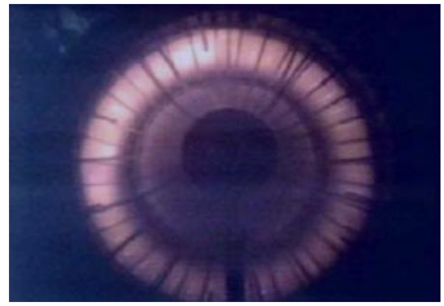

Figure 16. Image from Probe [42]

These probes have proven to last many years and thousands of hours at these elevated operation temperatures and mass flows behind turbine engines; however, it is not completely uncommon for failures to occur. These failures tend to occur almost exclusively because of cooing water issues. Some cooling water issues to be noted are debris clogged strainers and cooling passages that limit water flow through passages, and high pressure water pump failures. In either case, these failures are ultimately a result of the onset of film boiling, and thus melting of the material.

Recent test and evaluation capability upgrades at AEDC have sparked interest in using these imaging probes to collect high enthalpy environment data inside of high temperature wind tunnels that simulate true temperature hypersonic flight environments. While it is unsure if these probes will be able to handle the high heat flux environment needed for these high temperature applications, the analysis herein attempted to determine the CHF limits of this simplified geometry. Regardless of a final determination to subject these periscope probes to hypersonic ground test environments, this investigation concluded with an analytical determination of heat flux limits this imaging probe design would be able to endure before failure.

3.2.2 PERISCOPE PROBE GEOMETRY

Simplified versions of the probe's sub-assembly sections were created in a three dimensional model and can be seen in Figure 17. The cooling passages are semi-circular in cross-section with radii ranging from 0.049 to 0.065 inches. There is a total of eight inlet and eight outlet cooling channels, and Figure 18 shows orientation of cooling channels around the annulus of the probe body.

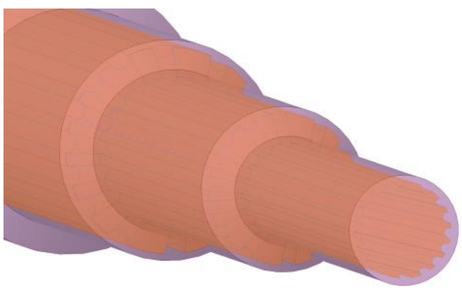

Figure 17. Imaging Probe Machined with Electroform Sheath

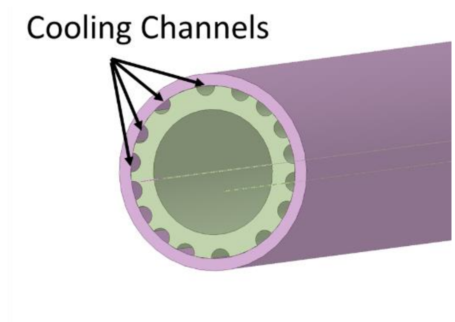

Figure 18. Cooling Channel Orientation

In application, there is a nitrogen purge channel which is omitted from this simplified modeled geometry. This purge is used in practice to cool purge the imagining lens for an installed camera and mirroring system. This investigation considers any extra benefits that might be gained from nitrogen purge in a localized area to be negligible. Also, structural effects from the camera viewing port were not considered in this model, and are considered secondary drivers to the thermal structural survivability that relates to the backside water cooling heat flux removal. The robust cooling system flows high pressure water in excess of 1,000 psia through small semi-circular cooling passages at high flow rates of up to 25 gpm (total system). For each individual cooling channel, the total flow rates are assumed to be equal with typical operational ranges between 0.2625 and 0.4375 lbm/sec. Figure 19 shows that for every single cooling passage supply there is a single return path.

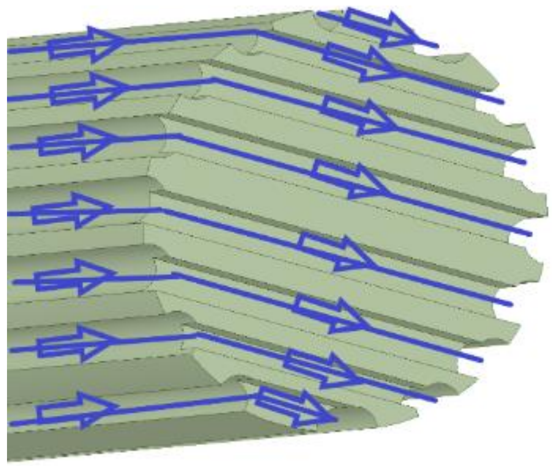

Figure 19. Imaging Probe Cooling Passages

The periscope probe's long length allows it to be penetrated into high enthalpy flows of up to over 50 inches of insertion depth. In most cases the probe is inserted into high enthalpy flows of no more than 20 inches, a typical operating practice behind turbine engine augmentors. The investigation herein focused on less than 16 inches of insertion depth where probe diameters are one and two inches in the two sections designated the focus area shown in Figure 20. This insertion depth chosen was based on the intended application in facility flow fields of interest, and even insertion depth was parametrically varied parameter for this investigation to enhance the operating CHF limits.

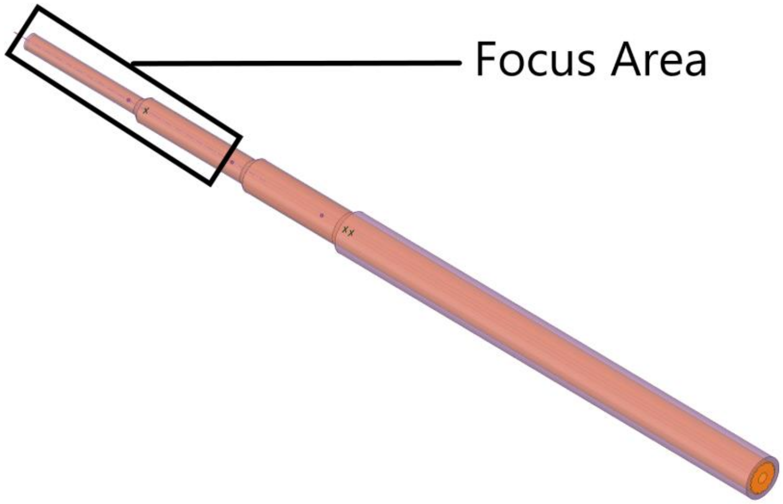

Figure 20. Imaging Probe Focus Areas

3.2.3 PROBE HISTORICAL HEAT FLUX OPERATIONS

Probe data has been collected from use behind turbine engines in afterburner operations where temperatures can exceed 3500 degrees Farhenheit. Also, there is data available from probe flow checks that were subjected to an oxygen-acetylene torch. In both scenarios, inlet and outlet cooling water temperatures and pressures were measured. These scenarios were used to anchor the values from the probe model generated in COOLWL for boiling predictions using Rohsenow nucleate boiling calculations. Data from the torch testing can be seen in Table 2, and torch testing station locations can be viewed in Figure 21. Because the input heat flux values from the torch testing were unknown, the data from this simple lab test was only used to make sure the COOLWL model was generating realistic results. It is important to note that the torch test was conducted as a means of hardware checkout, and was not a controlled experiment as part of this investigation.

Table 2. Torch Test Data

Torch Test at 500 psi	
Location	Max Temp, °F
1	73
2	70
3	70
4	70
5	70
6	70
7	70
8	68
9	70
10	70
11	70
12	70
13	70
14	70
15	70
16	66
17	70

Torch Test at 1,000 psi	
Location	Max Temp, °F
1	76
2	71
3	72
4	70
5	70
6	72
7	70
8	70
9	70
10	68
11	68
12	68
13	68
14	68
15	68
16	68
17	68

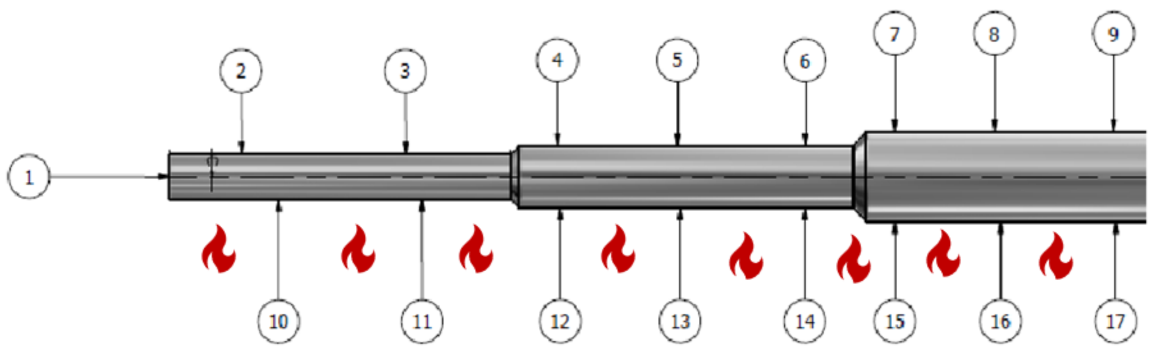

Figure 21. Torch Test Locations

4.0 APPROACH

4.1 OUTLINE OF APPROACH

The following is an outline of the approach used in this research investigation. Figure 22 shows the analytical process taken to arrive to determination of survivability. This process can be applied to many applications of fluid cooled structures in high heat flux environments.

- Step 1: Determination of peak heat fluxes of interest
  - Determination of relevant use cases
  - CFD simulation with different diameters/sections of cylindrical probe
  - Constant wall temperature assumed (initial estimation)
  - CFD Code: Wind-US circa 2013, using L-V equilibrium air
- Step 2: Insertion of peak heat fluxes (obtained from CFD) into COOLWL for determination of CHF and heat transfer coefficients
  - Simulation with probe dimensions and operation specifications
  - Parametric analysis varying water pressure, mass flux, and temperatures to improve CHF limits and optimize thermal performance
  - COOLWL code version: 2004
- Step 3: Ansys FEA model thermostructural survivability determination
  - Model generation of representative probe geometry in CAD software
  - Parametric analysis simulation of heat loads
    - Outer surface applied with peak heat flux from CFD
    - Computed heat transfer coefficients and surface temperatures used from COOLWL output
  - Ansys version: 2020 R2, using tetrahedral mesh

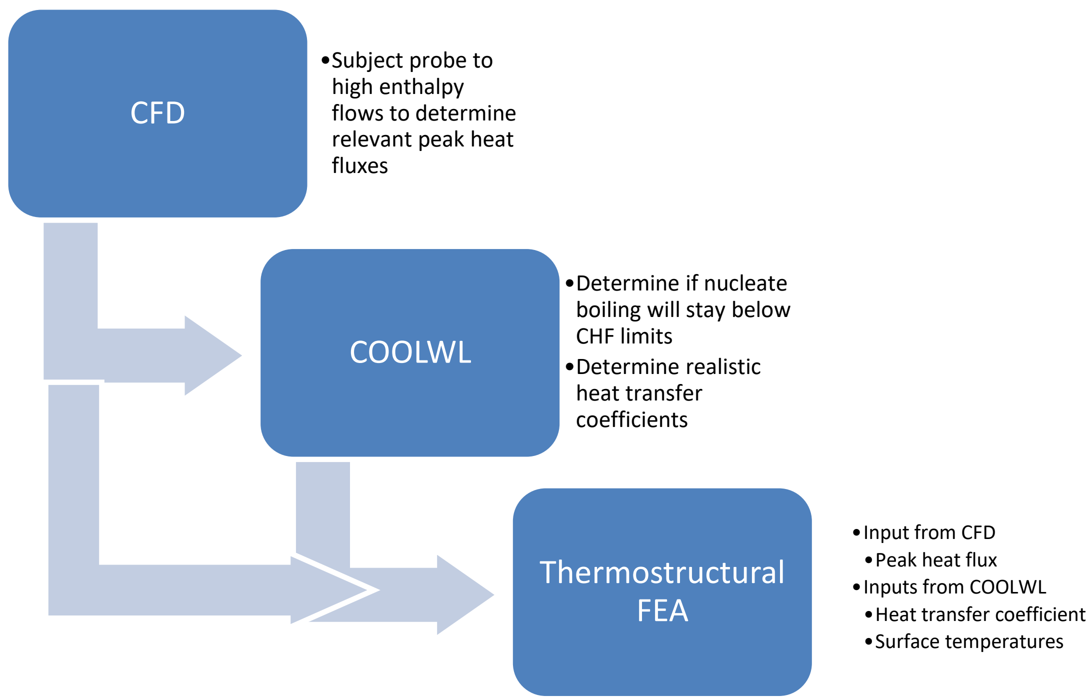

Figure 22. Survivability Investigation Approach Step Down Process

- Survivability criteria for this application
  - COOLWL - once CHF was reached, assumed probe failure
  - Thermostructural FEA – confirm survivability at peak heat flux loads
  - No specific factor of safety was used for this analysis
    - Conservative approaches were taken when applicable
    - For risk reduction, a factor of safety of 1.5 could be applied throughout the analysis to increase survivability confidence
- Presentation of Final Results
  - Parametric analysis of cooling fluid mass flux, subcooling, and pressure resulting in thermal performance optimization of the system
  - FEA thermostructural survivability results from ANSYS

- Final prediction of max heat flux conditions that the probe will survive, and recommendations for three supplied high heat flux use cases

4.2 DETERMINING REPRESENTATIVE HEAT FLUXES

The first step in investigating this problem was to determine possible realistic maximum heat fluxes on the probe geometry in relative high enthalpy flows. To determine peak heat fluxes, certain flow conditions were assessed to determine the air velocity, temperature, and pressure, and then these conditions were input in to a two-dimensional CFD simulation. Exact flow conditions used are not detailed in this document to adhere with DoD limited distribution directives; however, an example setup of the periscope probe in the simulation environment high temperatures and pressures can be seen in Figure 23 and Figure 24 respectively. Nevertheless, the basis of this study was focused on the values of peak heat fluxes entering into the probe structure, and this CFD was just a basis to determine potential peak heat fluxes. Omitting the CFD flow conditions and values does not take away from determining maximum heat flux survivability predictions included in this investigation. It is only discussed in this section to show the methodology used that can be applied to other thermostructural survivability use cases of interest.

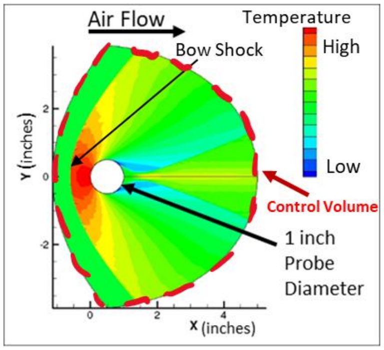

Figure 23. CFD Temperature Profile One Inch Diameter Section

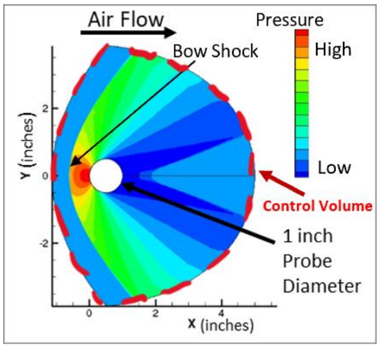

Figure 24. CFD Pressure Profile One Inch Diameter Section

Three realistic flow conditions of interest were chosen to determine peak heat fluxes that the cylindrical probes might encounter. A few basic assumptions were needed to setup the simulations. First off, the simulations were performed on two different diameter sections of the periscope probe. One section was a one inch diameter annulus which represents the smallest section towards the tip of the probe, while the other section had a two-inch diameter annulus and is the next smallest diameter section of the probe (see Figure 20). These sections were chosen based off of realistic use cases that the periscope probes might need to endure. Another assumption in these computations is that wall temperature was assumed to be constant. A constant wall temperature of 400 degrees Fahrenheit was used in these conditions. This temperature magnitude was only a starting point to get initial heat flux values of interest. There is an iterative process that is possible using the heat transfer coefficient equations from the boiling correlations and computing wall surface temperature. Using this process described in the results, see section 5.1, will enable convergence on a more closely matched initial wall temperature value.

The three conditions assessed were at different mass flows, pressures, and temperatures. The evaluation of the three conditions resulted in different peak (Q_{max}) and average (Q_{avg}) heat flux values. Two probe diameters (D) were assessed at these three different "case" conditions described in Table 3.

Table 3. Use Case Parameter Description

Parameter	Case #1	Case #2	Case #3
Temperature	Low	Medium	High
Pressure	High	High	Low

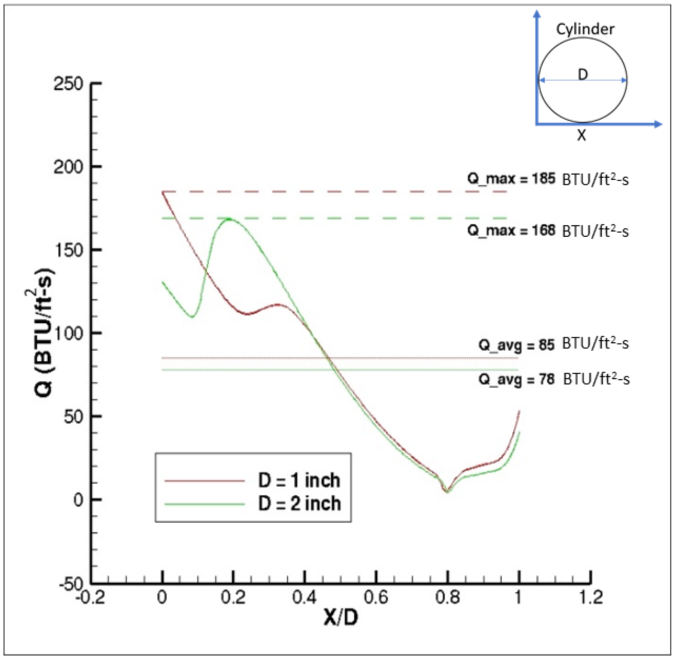

Figure 25. CFD Results Peak Heat Flux Case #1

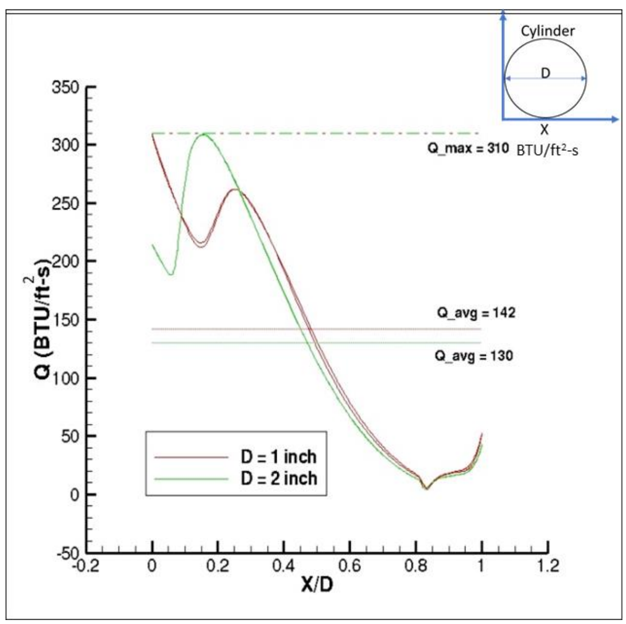

Figure 26. CFD Results Peak Heat Flux Case #2

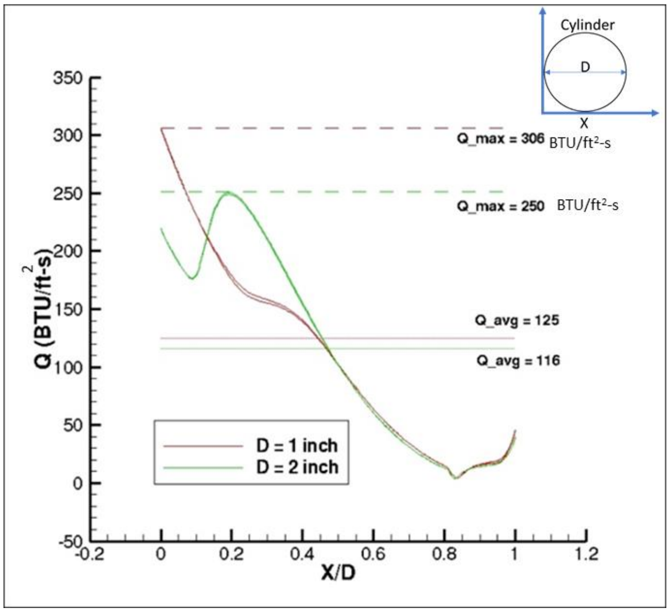

Figure 27. CFD Results Peak Heat Flux Case #3

The peak heat flux conditions of interest for this investigation were determined to range from 185 to 310 BTU/ft^2-s (0.210 to 0.352 kW/cm^2). This range of values was a starting point in the CHF correlations assessed with the COOLWL code.

4.3 COOLWL CORRELATIONS TO DETERMINE CHF

This section will detail how the CHF was predicted for the use cases as well as variations of nominal operating conditions that helped determine operation limits to ensure probe survival. First a description of how the COOLWL code used inputs to setup forced convection flow boiling for the configuration. Figure 28 shows a two-dimensional cross section of some inputs to aid in orientation, in which steady state Fourier heat conduction is performed through the 'wall to channel gap' distance specified. In this investigation the gap distance is 0.125 inches.

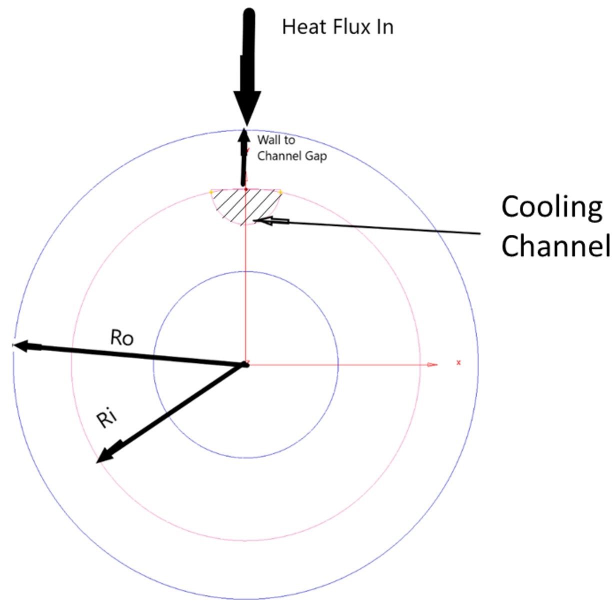

Figure 28. Two Dimensional COOLWL Input Probe Cross Section

Figure 28 highlights several variables that are inputs into the COOLWL code, where the single cooling channel has dimensions of area and hydraulic diameter. Length of this cross section can be extended by any specified value, where certain parameters can be varied along the length in specified intervals including the two dimensional cross section parameters shown in Figure 28. However, for the analysis herein the cross sectional parameters were constant the entire length, to include a continuous heat flux input to simulate the worst case scenario.

The other important configuration variables input into the COOLWL model were fluid flowrate, inlet fluid temperature, inlet fluid pressure, and probe material. Nickel was chosen as the material input which has effects in the Fourier conduction and Rohsenow boiling formulations. Table 1 (Section 2.2.2) was used to identify the experimentally determined surface to fluid coefficient ($C_{s,f}$) for the Rohsenow boiling correlation.

The length of probe subjected to peak heat fluxes was assumed to only be applied to the hotter side of the probe (upstream). This assumption was used in this CHF analysis based on knowledge of the conservative use cases, and results from the CFD analysis in Section 4.2, which determined the heat fluxes subjected to the colder side (downstream) to remain in heat flux ranges of 0 to 50 BTU/ft^2-s. This assumption would have to be implemented during setup and use of this probe in such a way that the cooling channel returns were positioned on the colder backside (downstream) of the probe.

After probe and cooling channel parameters were defined, the next step was to determine which forced convection and boiling calculations to use. For the forced convection computations, a comparison was made between the Colburn, Sieder-Tate, and Carpenter forced convection formulas from Equations 3, 4, and 5. The Petukhov forced convection equation (Equation 6) was not used for this comparison as the Reynolds number ranges for this situation were below the recommended range of at least above 10,000. While this cooling probe application does consist of turbulent flow, it deals with Reynold's number ranges around 7,000 to 10,500, thus justification for not including the Petukhov equations in the comparison. Even though it was not applicable to these use cases, it is still recommended to consider Petukhov's formulations in highly turbulent flow with Reynolds numbers in excess of 10,000.

A comparison of Colburn, Sieder-Tate, and Carpenter calculations were performed over the range of interested heat fluxes and typical operating parameters of 70 degree Fahrenheit cooling water inlet temperature, 1,000 psia inlet water pressure, and with a probe insertion depth of 8 inches. This boiling prediction comparison can be seen in Figure 29. This prediction was made in heat flux increments of 100 BTU/ft^2-s, and boiling incipience was reached before the first 100 BTU/ft^2-s increment in all three methods. Once boiling incipience was reached, Rohsenow's nucleate boiling correlation was to determine the boiling curve.

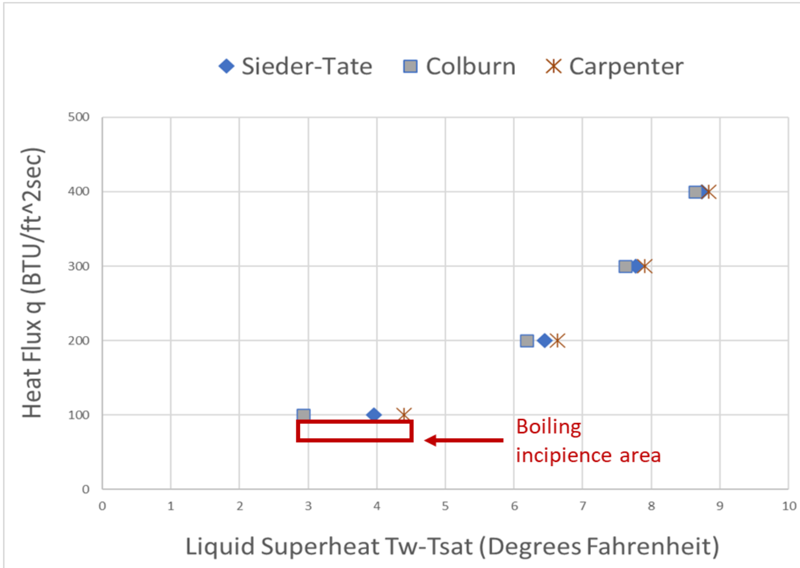

Figure 29. Nominal Conditions Sieder-Tate vs Colburn vs Carpenter

The Colburn, Sieder-Tate, and Carpenter predictions were then compared over different inlet water pressure conditions. Pressure effects are largely beneficial going from 500 to 1,000 psia, but then benefits started to diminish in magnitude due to saturation pressure and temperature properties of water. However, it is still beneficial to increase the saturation temperature of the bulk fluid above 1,000 psia. Pressures as high as 2,000 psia were considered for this application. Figure 30, Figure 31, and Figure 32 show pressure effects on the Colburn, Sieder-Tate, and Carpenter predictions, again with all three using Rohsenow's boiling correlation after incipience. Pressures in the 1,500 to 2,000 psia range indicated that boiling incipience would occur at some point after heat fluxes of 100 BTU/ft^2-s, and thus the points below 200 BTU/ft^2-s are not shown for these conditions.

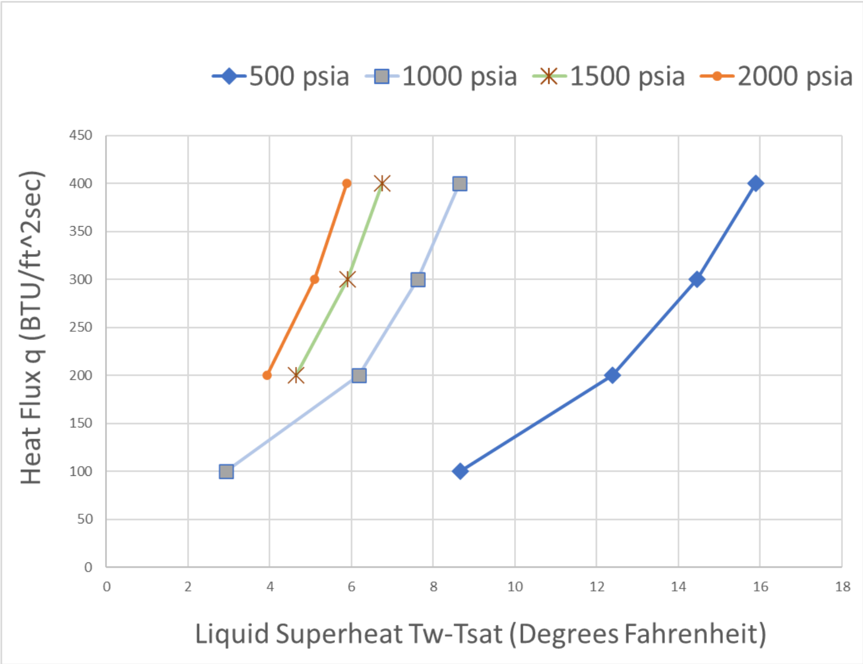

Figure 30. Pressure Effects on Colburn Predictions

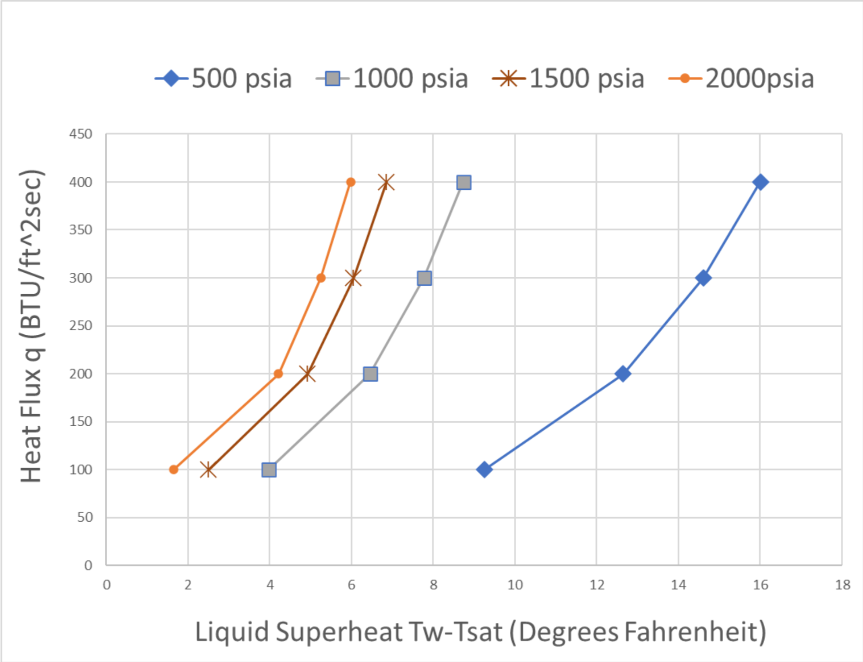

Figure 31. Pressure Effects on Sieder-Tate Predictions

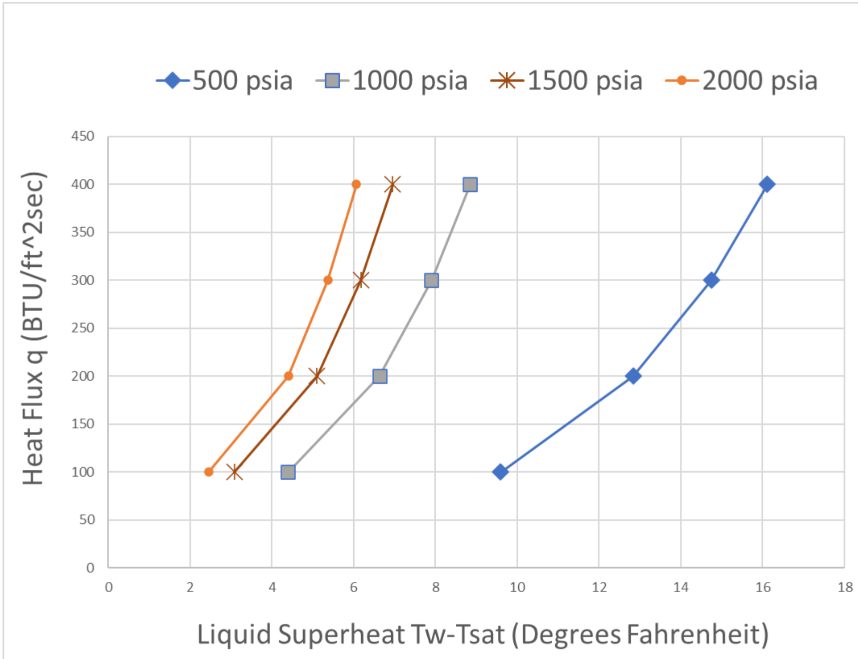

Figure 32. Pressure Effects on Carpenter Prediction

Table 4 shows the values of heat flux for the Colburn, Sieder-Tate, and Carpenter predictions at the start of boiling incipience over the range of pressures. As a conservative approach, it was decided from this point forward to only compare the Sieder-Tate and Carpenter predictions as the Colburn boiling incipience predictions were consistently high when compared to the other two. Then, a comparison was made between the Sieder-Tate and Carpenter calculations at different water inlet temperature conditions of 50, 100, and 150 degrees Fahrenheit at a normal operating pressure of 1,000 psia. This inlet temperature comparison can be seen in Figure 33 as the predictions of different boiling incipience points are calculated.

Table 4. Start of Boiling Incipience Correlation Comparison

Boiling Incipience (BTU/ft^2sec)				
Pressure	**500 psia**	**1000 psia**	**1500 psia**	**2000 psia**
Colburn (BTU/ft^2sec)	54.4	88.6	105.9	115.8
Sieder-Tate (BTU/ft^2sec)	44.3	71.3	85.6	94.1
Carpenter (BTU/ft^2sec)	37.8	60.9	73.1	80.3

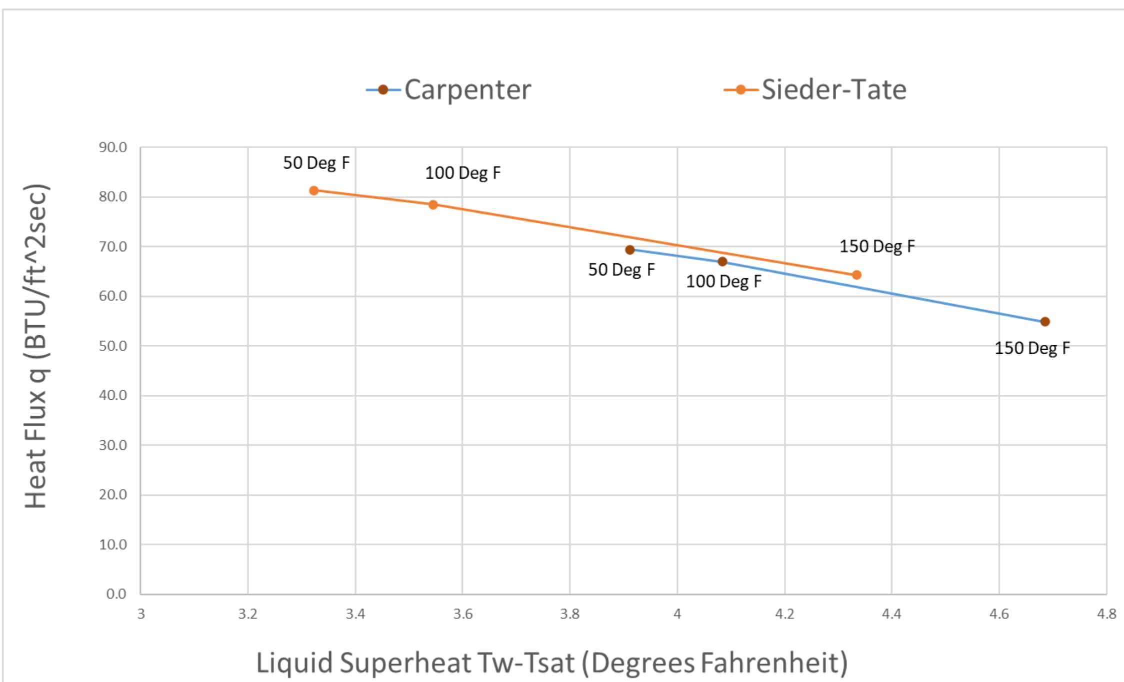

Figure 33. Inlet Temperature Effect on Boiling Incipience

One last comparison was made between boiling incipience and a variation of mass flow. It was determined when mass flow values were increased, the boiling incipience points increased as well. This is as expected because boiling can be combated by increasing the mass flux which allows for the bubbles to sweep away from the wall and the bulk fluid to reattach to the wall. These comparisons are in Table 5 and were conducted using the 8-inch length, at 70 degrees Fahrenheit, and 1,000 psia.

Table 5. Boiling Incipience at Different Mass Flows

Boiling Incipience (BTU/ft^2sec)				
	Mass Flow			
	0.2 lbm/sec	**0.3 lbm/sec**	**0.4 lbm/sec**	**0.5 lbm/sec**
Sieder-Tate (BTU/ft^2sec)	44.0	57.6	68.2	75.7
Carpenter (BTU/ft^2sec)	37.5	49.1	58.1	64.6

Now that a model of the periscope probe configuration was setup in COOLWL, the next step was to analyze results using CHF correlations discussed from Section 2.5. Although not critical, the Carpenter et al. [29] boiling incipience calculations were used in the remainder of this investigation, where the approach was to compare the nominal probe configuration across relevant CHF correlations at different insertion depths and heat flux ranges of interest. Then a parametric analysis was completed to optimize the thermal performance of the system. See results Section 5.1 for CHF analysis.

4.4 THERMOSTRUCTURAL SURVIVABILITY

The last step to determine thermostructural survivability was to generate a simplified model of two cooling channels located at the periscope probe tip. This model was generated to determine if thermal stress and strain would reach material limits of the nickel electroformed shell. To simplify the analysis, the two sections of stainless steel and nickel were joined together and analyzed as a single structure using the properties of nickel. This simplified section can be seen in Figure 34. Various versions of meshing were used, and a non-linear mechanical mesh can be seen in Figure 35.

A complete FEA structural analysis to include flow conditions from CFD were not the focus of this investigation; however, steady state thermal and static structural analyses were completed. The steady state thermal analysis consisted of applying a constant heat flux (310 BTU/ft^2-s) to the outer surface seen in Figure 36.

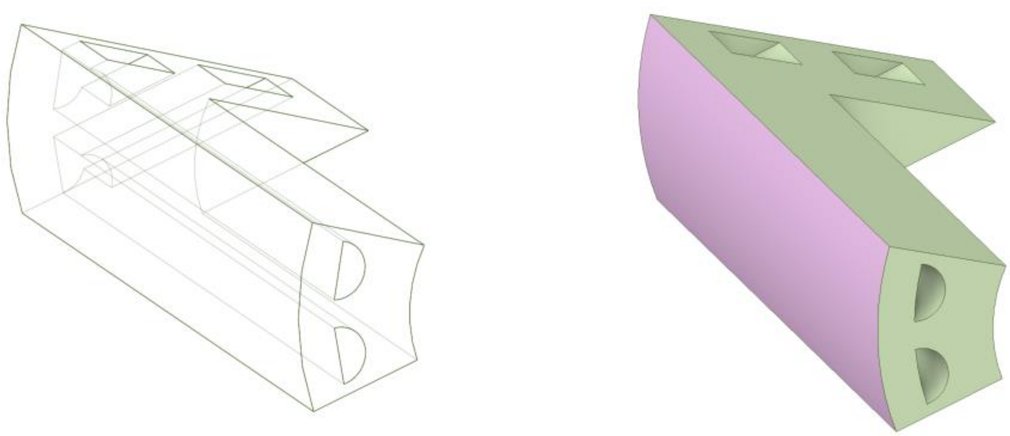

Figure 34. Two Cooling Channel Simplified Model

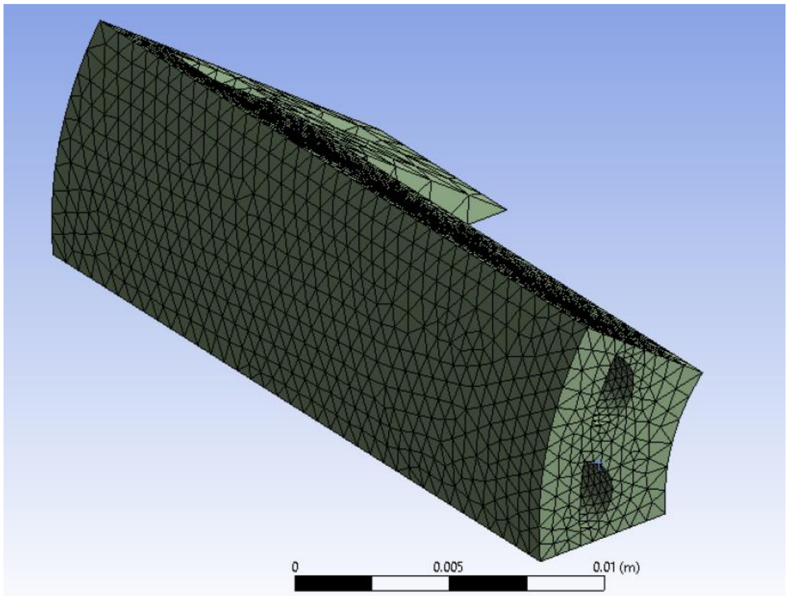

Figure 35. Model Mesh

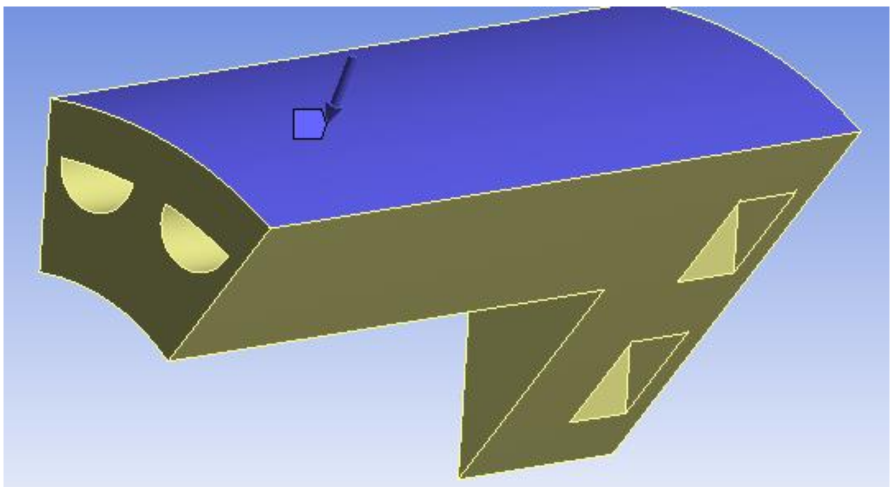

Figure 36. Applied Heat Flux Load

Next a constant forced convection load was applied inside the cooling channels and was set as the outputs from COOLWL using the Rohsenow {19] nucleate boiling predictions. These COOLWL predictions also supplied the heat transfer coefficients used for the convection load, which were called “Film Coefficient” in ANSYS. Temperature boundary conditions were set on the semicircular section of the cooling channels, and were representative of the bulk fluid temperatures as resulting from the Rohsenow boiling calculations. The Ansys model convergence criteria was set to default, which uses the Newton's Raphson method for convergence.

Strategy for implementing an FEA thermostructural analysis was not only to ensure probe survivability, it was also to allow for convergence of wall temperatures and heat transfer coefficients. The initial values input into CFD to determine peak heat flux loads of interest included an assumption of constant wall temperatures. While the assumption of 400 degrees Fahrenheit was a good starting point, it allowed the iterative process to get underway. This thermostructural analysis is the last step before the process of heat transfer coefficient and wall temperature convergence. The resulting wall temperature from the FEA, allows the value to be updated into the initial CFD model. Then CFD will update the applicable load into COOLWL, where COOLWL will then update the load and coefficient inputs into the thermostructural analysis, and so on. This iterative process is not followed out completely in this investigation as the emphasis was on the investigation of CHF; however, this investigation discovered this useful iterative process during the CHF correlation effort. This heat transfer coefficient converging process can be visualized in Figure 37.

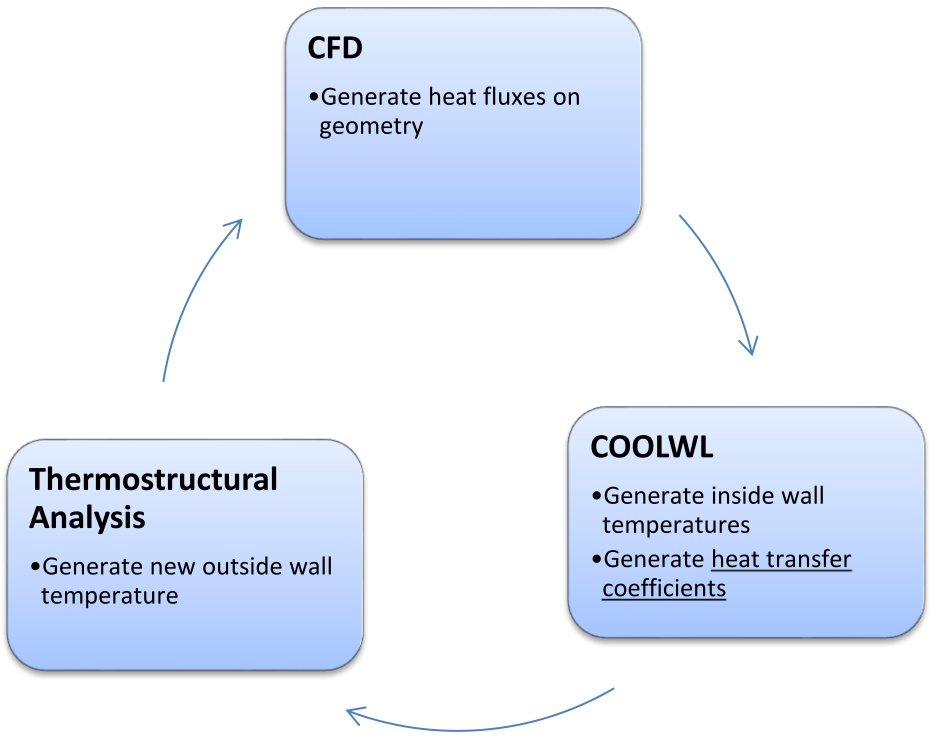

Figure 37. Heat Transfer Coefficient Convergence Process

4.5 SURVIVABILITY CRITERIA

This section describes the approach taken on how to apply the appropriate CHF correlations to the model generated in COOLWL, and on how outputs of the boiling correlation code were applied to the FEA thermostructural analysis. First, the determination of what CHF correlations to use were determined from literature review; however, some of the CHF correlations chosen were not a good fit for this application and this was not obvious until it was applied to the model generated in COOLWL. The following correlations were determined from literature to be the most applicable to this cooling probe scenario.

- Bernath [37]
- Levy [38]

- Vandervort, et al. [40] (determined to be outside of applicable range)
- Van Huff and Rousar [as cited in Beitel 2]
- Labuntsov [39]
- Rohsenow [19] nucleate boiling correlation

The Rohsenow correlation was utilized to setup the model for the periscope probe as shown in Section 4.3. The Vandervort et al. correlation was initially selected because of its reported success; however, after troubleshooting it was determined that this promising correlation was not applicable to the periscope probe configuration. Originally all parameters looked to be within the probe application range of interest except for $\frac{L}{D}$. Unfortunately, because $\frac{L}{D}$ is on the wrong side of the only subtraction function in the correlation, and when the term gets much bigger than 40, it results in multiplication of a negative value. Thus, the Vandervort et al. correlation must be close to the $\frac{L}{D}$ range of 1 to 40 for a valid calculation. The main driver in this is not cooling channel sizes themselves, but the analysis technique of only assessing one cooling channel. If a smaller length section were assessed and multiple channels were evaluated at the same time, then the $\frac{L}{D}$ term would become small enough to be within the range in which Vandervort et al. correlations could be applied.

Nevertheless, the first step was to use Bernath, Levy, Van Huff and Rousar, and Labuntsov correlations to determine CHF points over a variety of parameter ranges. This assessment was done over a length of cooling channel section, to determine how much, if at all, the probe would be able to be inserted into the flow field. The method used to determine the length of probe that would be below CHF values can be seen in the generic sample in Figure 38. This method determined that once correlation CHF prediction falls below the applied heat flux value, then the probe was predicted to have reached CHF.

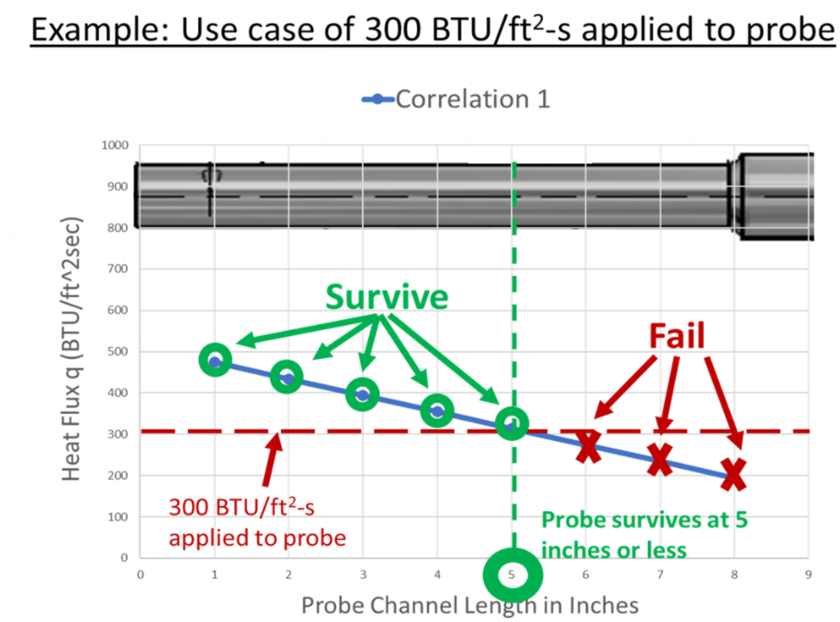

Figure 38. Sample CHF Survival Explained

The next step was to use the wall temperature, bulk fluid temperature, and heat transfer coefficient values from the Rohsenow correlation and input them into an FEA thermostructural model. While the CHF will look at a wide range of operating conditions to best understand the cooling abilities of the configuration, the FEA thermostructural analysis will look at the worst case scenario and work down from there only if applicable. Specifically, the FEA analysis can survive the worst case determined from the CHF analysis, then there is no need to look at other less extreme cases. Lastly, the thermostructural analysis defined an updated outside wall temperature which could be used to converge the heat transfer coefficients by first updating the CFD predictions and then COOLWL.

5.0 RESULTS

5.1 CHF

The major correlations used were Bernath, Levy, Van Huff and Rousar, and Labuntsov. First, the CHF was assessed at nominal operating conditions of the periscope probe, which has historically been at 1,000 psia, 70 degrees Fahrenheit, with a mass flow of 0.2625 $\frac{lbm}{sec}$ per cooling channel. However, it is not uncommon to run with pressures ranging from 500 to 1,500 psia, inlet temperatures from 50 to 90 degrees Fahrenheit, and flow rates as high as 0.4375 $\frac{lbm}{sec}$ per channel. As a starting point, the nominal operating condition was subjected to a conservative 400 BTU/ft^2-s for the entire eight inch length, and the results for those four CHF correlations can be seen in Figure 39. The value of 400 BTU/ft^2-s was used initially as a quick assessment and as a conservative value that would provide some safety margin for operations at maximum heat flux condition of 310 BTU/ft^2-s.

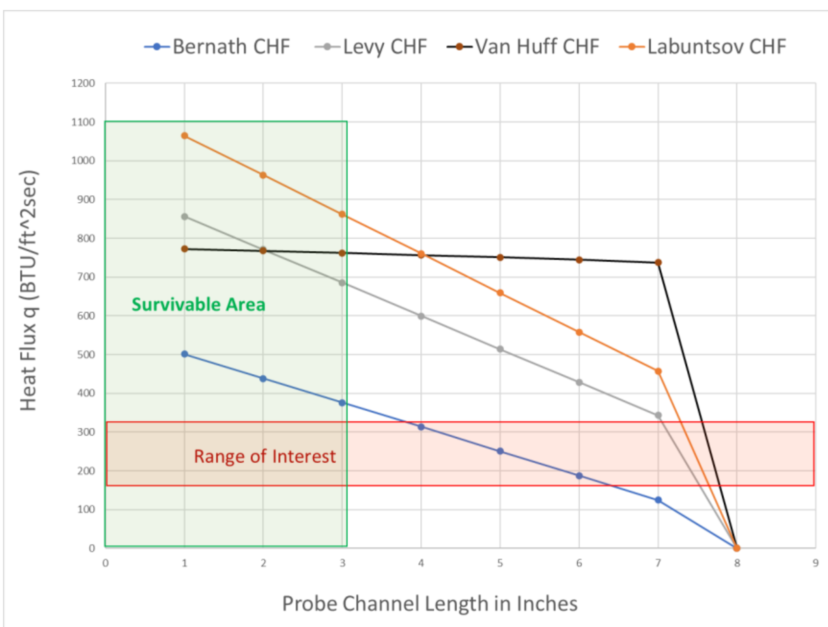

Figure 39. CHF Nominal Probe Configuration

The nominal probe configuration CHF correlations showed promising results. Even though only three inches for all the correlations were below the CHF values, it predicted that at least three inches would survive in the flow, and that was before optimization attempts. So, even if no other optimizations were possible, predictions were that the camera probe would survive while inserted no more than three inches in the flow at normal operating conditions subjected to 400 BTU/ft^2-s along the length.

Going forward with the investigation, the Bernath correlation was used as the main CHF determination prediction. Not only was the Bernath correlation chosen because of the relevance of small hydraulic diameters, but it was also the most conservative correlation of the four chosen for this investigation.

5.1.1 CHF AT CONDITIONS OF INTEREST

The range of historical operations were explored to see if the CHF values at other possible operating conditions would improve the predictions to allow more length of the probe inserted into the flow. First it was determined from literature that velocity had a significant impact on nucleate boiling and CHF values, so the nominal operating mass flow conditions were increased to 0.4375 $\frac{lbm}{sec}$ in the CHF prediction model. This higher flow rate has been proven through bench testing, and Figure 40 shows this condition while being subjected to the conservative heat flux of 400 BTU/ft^2-s. This resulting simulation predicted that the probe could survive in the flow with up to five inches of insertion.

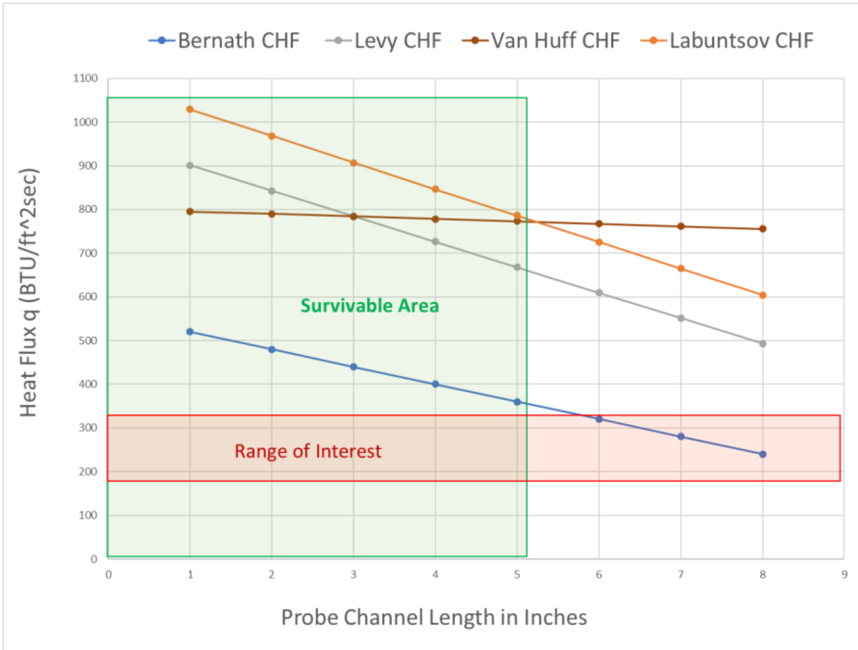

Figure 40. CHF Prediction at Increased Velocity

The flow rates from bench testing (not shown herein) that achieved the higher flow rate values of 0.4375 lbm/sec were utilizing a pump that only provided 800 psia at the entrance of the probe housing. So, the same conditions were simulated again but the pressure was reduced from 1,000 psia to 800 psia, and these results can be seen in Figure 41. The decrease in pressure changed the prediction to only 4 inches of insertion. Figure 42 shows the same case as Figure 41, but with the max use case conditions of 310 BTU/ft^2-s applied across the probe surface instead of the conservative value of 400 BTU/ft^2-s. This resulted in a prediction of 6 inches of insertion depth.

Figure 43 shows the same conditions except with 200 BTU/ft^2-s applied across the probe surface to show the possibilities of probe insertion depth at lower heat flux conditions. The insertion depth increased to fourteen inches at heat fluxes of 200 BTU/ft^2-s or below.

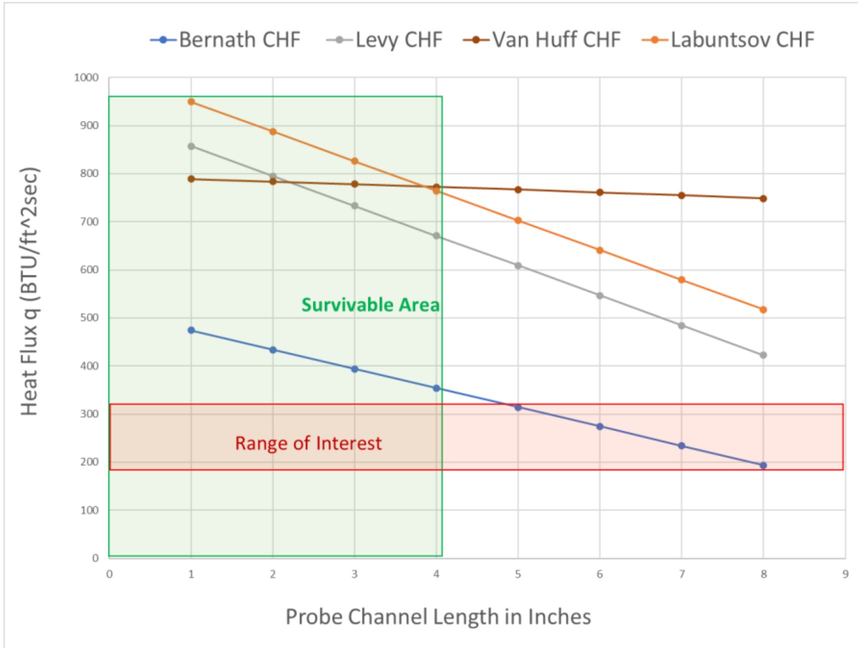

Figure 41. CHF Increased Velocity with Historical Pressure data

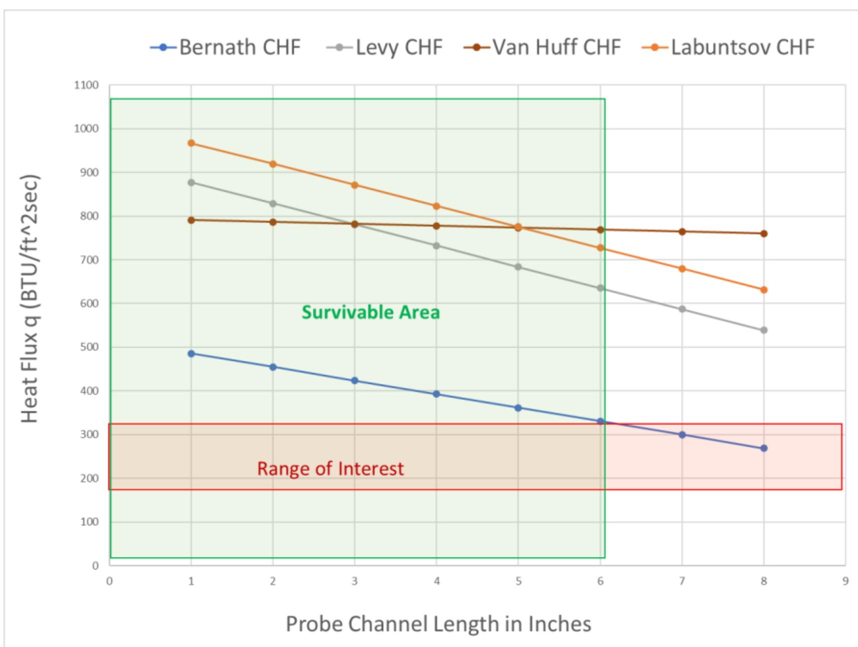

Figure 42. CHF at 310 BTU/ft^2-s Conditions

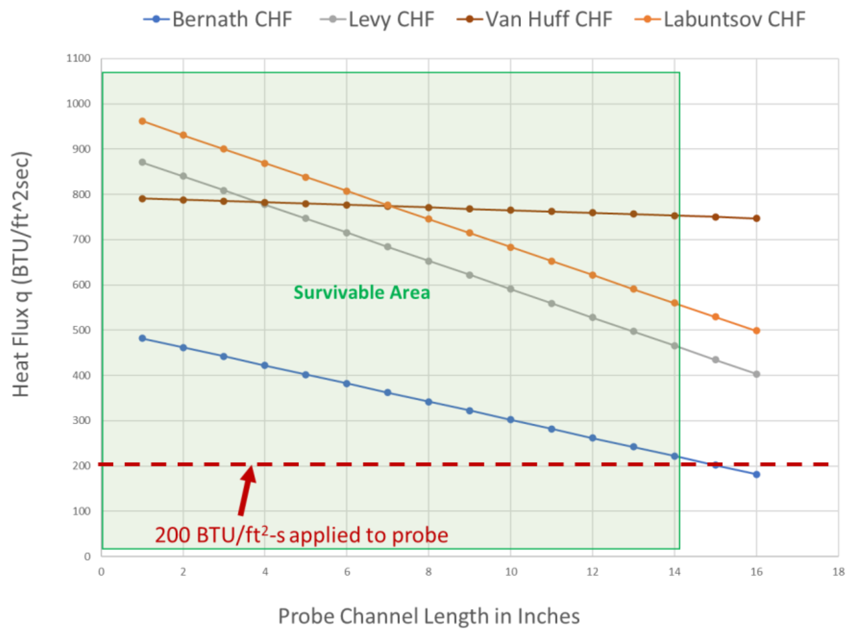

Figure 43. CHF at 200 BTU/ft^2-s

5.1.2 THERMAL PERFORMANCE OPTIMIZATION OF CHF

This section details optimization of the adjustable parameters within this configuration within realistic limits. Figure 44 shows the conservative case of 400 BTU/ft^2-s applied to the probe with an increase of cooling water operating pressure to 1,500 psia, while Figure 45 shows an increase in cooling water operating pressure up to 2,000 psia. The two figures are directly comparable to the 800 psia case from Figure 41. There was not much gained (one inch insertion) in going from 1,500 psia to 2,000 psia (7 to 8 inches respectively). It was determined to utilize the optimization of 1,500 psia conditions, because readily available pumping systems already exist to get these conditions at flowrates specified.

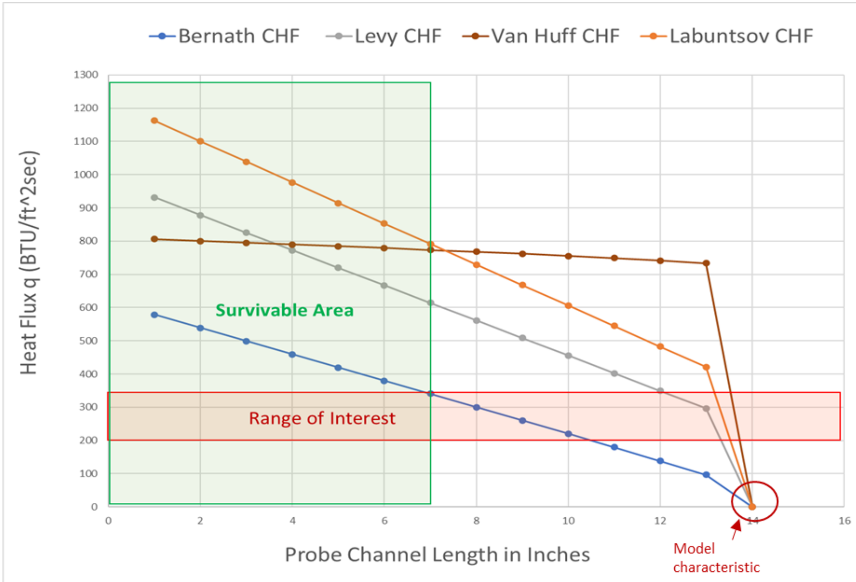

Figure 44. CHF Optimized at 1,500 psia

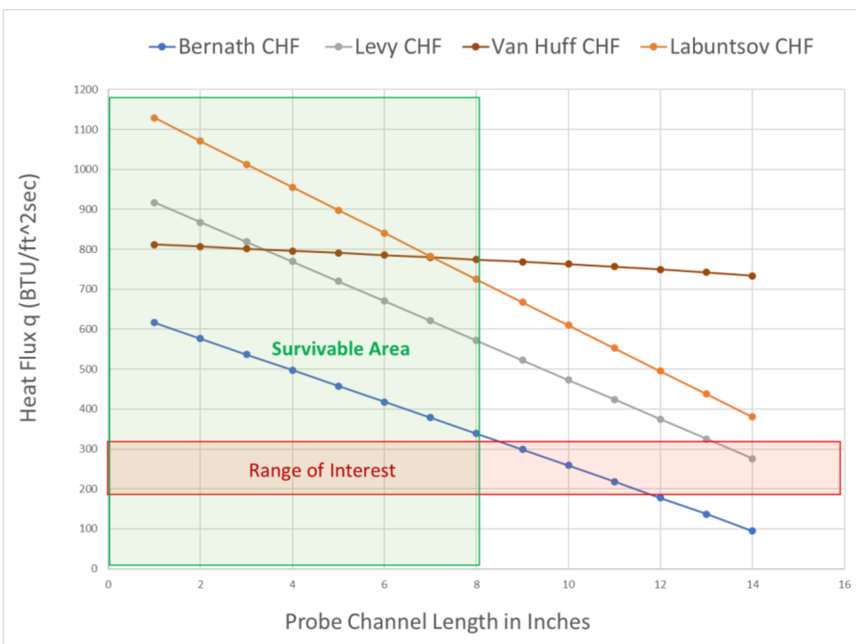

Figure 45. CHF Optimized at 2,000 psia

Temperature effects of the 400 BTU/ft^2-s conservative case was assessed using only the Bernath CHF correlation at 1,500 psia. Temperature has an effect going from 50 to 150 Degrees Fahrenheit and these affects can be viewed in Figure 46. However, for optimization of the system it is recommended to run at cold ambient conditions, and no ancillary system installed to pre-chill cooling water. Such a system would be too costly and provide little benefit in this application. Furthermore, inlet temperatures should be monitored real-time during operations, and in the event inlet temperatures reached 100 degrees Fahrenheit, that might result in having to pull the probe up to an inch out of the flow. Likewise, if colder temperatures were available such as in winter months, then it might be possible to move the probe further into the flow by up to one inch.

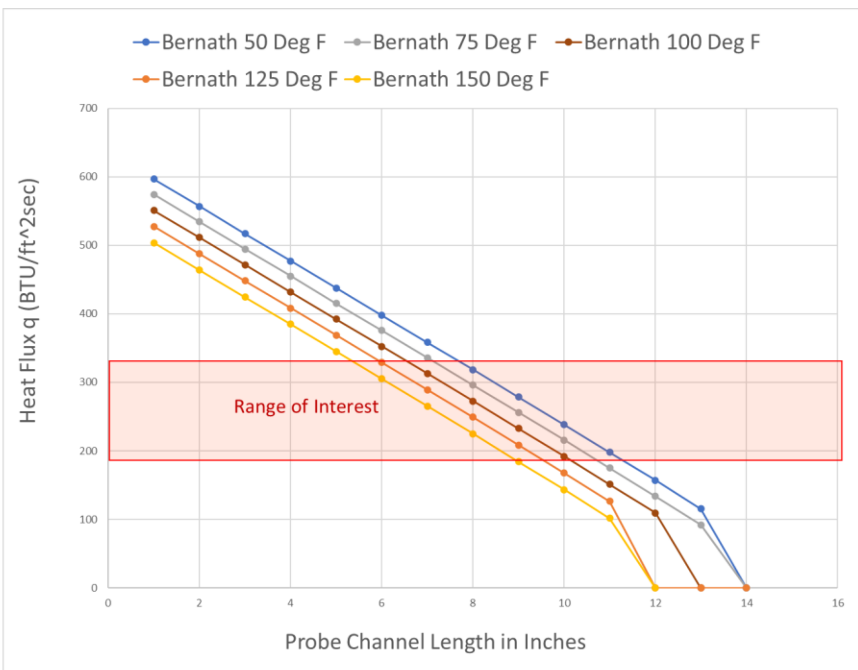

Figure 46. CHF Temperature Effects

Mass flow was already parametrically assessed in Section 5.1.1, and determined that the maximum mass flow condition for this probe should be utilized. Next, the optimized probe cooling water configuration of 1,500 psia at 0.4375 $\frac{lbm}{sec}$ was applied to the maximum use case of 310 BTU/ft^2-s, shown in Figure 47. This resulted in a maximum depth of nine inches at operating parameters specified.

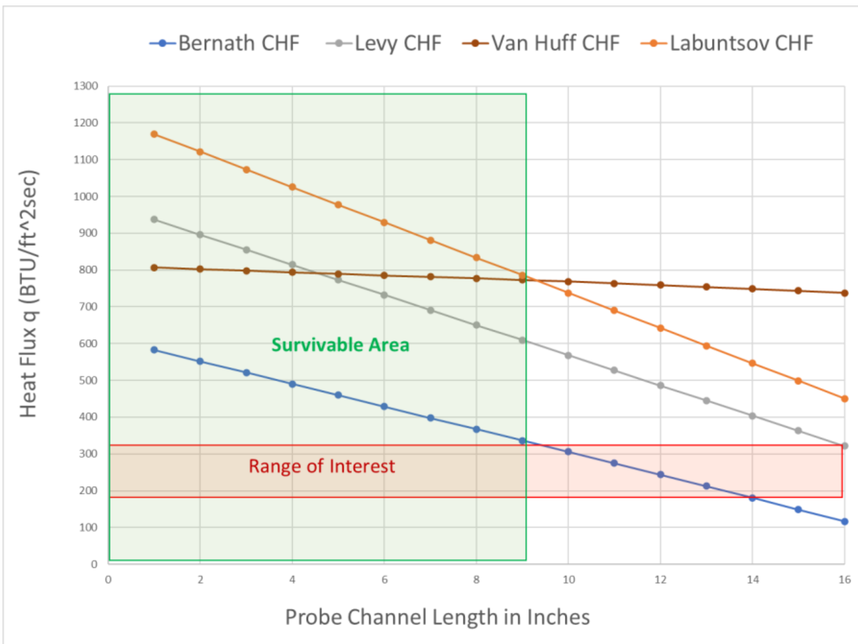

Figure 47. Maximum Insertion Depth at 310 BTU/ft^2-s

Maximum heat flux conditions the probe could survive was then applied to the Bernath correlation over a range of heat fluxes seen in Figure 48. This indicated that probe survivability could be possible at heat fluxes up to 500 BTU/ft^2-s at an insertion depth of two inches.

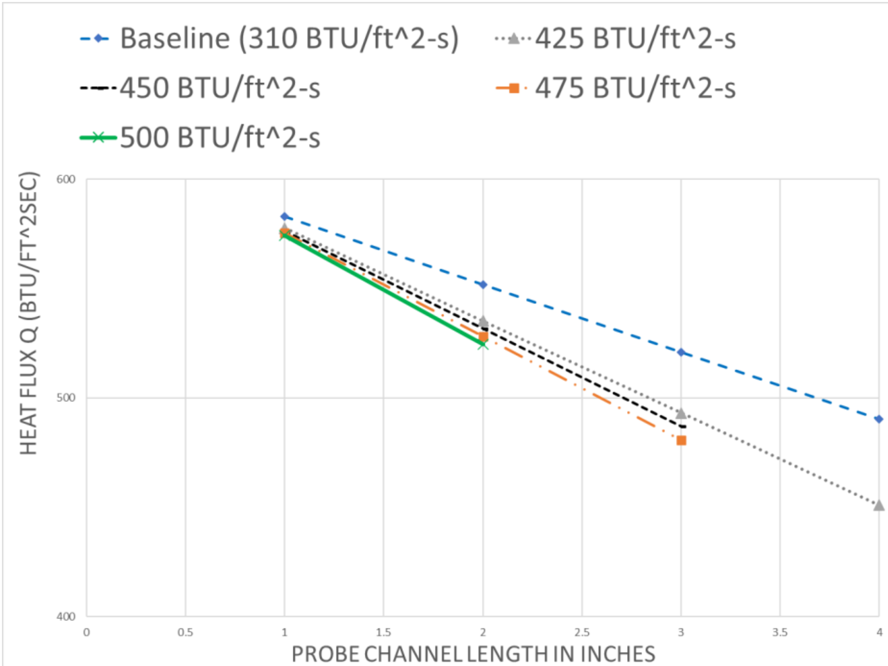

Figure 48. Maximum Heat Flux

5.2 THERMOSTRUCTURAL ANALYSIS

At the maximum heat flux condition of use cases (310 BTU/ft^2-s), simplified thermostructural model showed thermal stresses within acceptable strength limits. The von-Mises stress calculations were relatively close to the tensile yield strength of nickel. While not part of this investigation, it can be suggested that more analysis of survivability can be determined from the thermostructural model to not only converge on updated heat transfer coefficients, but also to input other parameters of interest such as flow conditions. The outside wall temperature varied from the original 400 degree Fahrenheit CFD estimate by more than 200 degrees. This large temperature difference highlights the need for a process to converge on heat transfer coefficients and wall temperatures. The new wall temperature would provide new predicted peak heat flux values in CFD that are lower than the original maximum value of 310 BTU/ft^2-s, which is a result of a lower temperature difference between the wall surface and the film temperature.

6.0 CONCLUSIONS AND RECOMMENDATIONS

The work included in this research and investigation has provided insight into the survivability predictions of an existing periscope imaging probe hardware. This work includes a model developed for the existing hardware to predict boiling incipience, nucleate boiling, and CHF conditions at various heat flux conditions and exposed lengths of the probe. The calculation of CHF was predicted using experimental correlations of similar parameter ranges for different use cases of interest. However, it is concluded that even closely related correlations provide a wide range of uncertainty, and the only true way to predict CHF on the hardware evaluated herein, is to assess the exact configuration in controlled experiments to failure points of CHF. To avoid this costly endeavor, CHF correlations from literature were used to provide confidence and operational boundary conditions for the periscope imaging probe at high peak heat flux conditions.

CHF predictions for the optimized operating parameters resulted in confidence that the probe could survive in the heat flux ranges of interest (180 to 300 BTU/ft^2-s) with an insertion depth of nine inches. Also, correlations predicted that operations in environments of 500 BTU/ft^2-s could be survivable with just two inches of the probe inserted into the flow.

The thermostructural FEA demonstrated that as long as cooling water stays below the limit of CHF, then the probe is structurally capable of surviving the heat flux environments of interest. However, a more detailed analysis could be conducted on the model to account for more parameters from the use cases, such as aerodynamic loading or cooling fluid pressures.

There were many limitations to this modeling effort, and further analysis in multiple areas could be conducted to further examine this probe hardware. It would be of benefit to assess the turbulent flow conditions in the cooling channels, especially towards the end of the probe where uneven flow distributions are probable. Another area of concern are shocks coming from upstream of this probe hardware that could create shock impingements on the probe structure, and thus stronger concentrations of localized heat flux on the surface of the probe. The survival of the probe in these high flow conditions could very well depend upon shock impingements. Another consideration to study is the orientation of the cooling channel to the flow. This investigation assumed the cooling channel was aligned perfectly facing upstream, however conditions where the cooling channel may not be perfectly aligned would be of interest and important to know during hardware installation.

If the hardware design went under a design revision, suggestions and considerations to analyze would be the electroform thickness, cooling channel size, and probe outside diameter size.

To finish, it is important to understand and monitor cooling water parameters for this imaging probe hardware being inserted in extreme heat flux conditions outside the bounds of which it has even been subjected. Pretest verifications will need to be conducted with "as installed" values loaded into the model for operational guidance on probe survivability. This investigation herein provides the analysis and process required to define the heat flux operating envelope of the periscope imaging probe; however, correlation values used have shown to previously have uncertainties has high as plus or minus 100 percent. As a consequence of high uncertainties in applying CHF correlations, conservative approaches were taken in many steps of the process as described herein.

LIST OF REFERENCES

1. Lee, C. H. and Mudawwar, I., "A Mechanistic Critical Heat Flux Model for Subcooled Flow Boiling Based on Bulk Flow Conditions," Int. 1. Multiphase Flow, Vol. 14, No.6, pp. 711-728, 1988.
2. Beitel, G.R., “Boiling Heat-Transfer Processes and Their Application in the Cooling of High Heat Flux Devices,” AEDC-TR-93-3, Arnold Engineering Development Center, Arnold Air Force Base, TN, June 1993.
3. Nukiyama, S. “The Maximum and Minimum Values of Heat Q Transmitted from Metal Surface to Boiling Water Under Atmospheric Pressure,” Translated in Int. J. Heat Mass Trans., Vol. 9, pp. 1419-1433, 1966.
4. Mudawar, I., “Technical Background: Boiling Advantage,” Mudawar Thermal Systems, West Lafayette, IN, 2009, http://www.mudawar.com/technical-bkgrnd/mts-boiling-advantage.php.
5. McAdams, W.H., “Heat Transmission”, 3rd Edition, McGraw-Hill Book Company, Inc., New York, NY, 1954.
6. Mattson, R.J., Hammitt, F.G. & Tong, L.S., “A photographic study of the subcooled flow boiling crisis in Freon-113,” ASME 73-HT-39, 1973.
7. Cichelli, M. T. and Bonilla, C. F. "Heat Transfer to Liquids Boiling Under Pressure." Transactions of the AIChE, Vol. 41, pp. 755-787, 1945.
8. Addoms, J.N. “Heat Transfer at High Rates to Water Boiling Outside Cylinders,” DSc Thesis, MIT, 1948.
9. Mishima, K., Hibiki, T., and Nishihara, H., “Effect of Pressure on Critical Heat Flux for Water in an Internally Heated Annulus,” The 4th International Topical Meeting on Nuclear Thermal Hydraulics Operations and Safety, Taipei, Taiwan, April 1994.
10. Katto, Y., "A Generalized Correlation of Critical Heat Flux for the Forced Convection Boiling in Vertical Uniformly Heated Round Tubes," Int. 1. Heat Mass Trans., Vol. 21, pp. 1527-1542, 1978.
11. Boyd, R. D., “Subcooled Flow Boiling Critical Heat Flux (CHF) and Its Application to Fusion Energy Components. Part I. A Review of

Fundamentals of CHF and Related Data Base," Fusion Technology, Vol. 7, pp. 7-30, January 1985.

12. Jabardo, J.M.S. "An Overview of Surface Roughness Effects on Nucleate Boiling Heat Transfer," The Open Transport Phenomena Journal, pp. 24-34, 2010.
13. Corty, C. and Foust, A.S. "Surface Variables in Nucleate Boiling," Chemical Engineering Progress Symposium Series, Vol. 51, No.17, pp. 1-12, 1955.
14. Kozitskii, V.I., "Heat Transfer Coefficients for boiling of n-butane on surfaces of various roughness," Chem. Pet. Eng., vol. 8, No. 1, pp. 23-24, 1971.
15. Nishikawa, K., Fujita, H., Ohta, and Hidaka, S., "Effect of roughness on the nucleate boiling heat transfer over the wide range of pressure," Seventh International Heat Transfer Conference, vol. 4, pp. 61-66, München, Germany, 1982.
16. Bergles, A.E., Morton, H.L. "Survey and Evaluation of Techniques to Augment Convective Heat Transfer," MIT Technical Report No. 5382-34, February 1965.
17. Leung, A., Banerjee, S., and Groeneveld, D.C., "Investigation of the Effects of Heater Characteristics on CHF Performance of a Long Vertical Annulus in High Pressure Water," 7th International Heat Transfer Conference, Vol.4, pp. 303-308, 1982.
18. O'Hanley, H.C., Coyle, C. Buongiorno, J. McKrell, T., Hu, L.W., Rubner, M., Cohen, R., "Separate Effects of Surface Roughness, Wettabillity, and porosity on the Boiling Critical Heat Flux," Appl. Phys. Lett. 103, no.2, 2013.
19. Rohsenow, W. M., "A Method of Correlating Heat-Transfer Data for Surface Boiling of Liquids," Trans. ASME, Vol. 74, pp. 969-975, 1952.

20. Vachon, R. I., Nix, G. H., and Tanger, G. E., "Evaluation of Constants for the Rohsenow Pool-Boiling Correlation," J. Heat Transfer, Vol. 90, pp. 239-247, May 1968.
21. Incropera, F. P., DeWitt, D. B., Bergman, T.L., and Lavine, A.S., "Fundamentals of Heat and Mass Transfer," 6th Edition, John Wiley and Sons, Hoboken, NJ, 2007.
22. Delvallem, V.H., Kenning, D.B.R. "Subcooled Flow Boiling at High Heat Flux," International Journal of Heat and Mass Transfer, Vol. 28, pp.1907-1920, October 1985.
23. Winovich, W., Carlson, W.C.A. "The 60-MW Shuttle Interaction Heating Facility, ISA Proceedings of the 25th International Instrumentation Symposium Instrumentation in the Aerospace Industry, Vol. 25, pp. 59-75, 1979.
24. Katto, Y., "A Physical Approach to Critical Heat Flux of Subcooled Flow Boiling in Round Tubes," Int. 1. Heat Mass Trans., Vol. 33, No.4, 1990, pp. 611-620.
25. Katto, Y., "Prediction of Critical Heat Flux of Subcooled Flow Boiling in Round Tubes," Int. J. Heat Mass Trans., Vol. 33, No.9, pp. 1921-1928, 1990.
26. Bergles, A.E. "Subcooled Burnout in Tues of Small Diameter," ASME 63-WA-182, ASME Winter Annual Meeting, Philadelphia, PA, November 1963.
27. Hughes, T.G., "Critical Heat Fluxes for Curved and Straight Surfaces During Subcooled Flow Boilng," PhD Thesis, Pennsylvania State University, TM-74-194 (ADA003036), June 1974.
28. Sleicher, C.A., Rouse, M.W., "A Convenient Correlation for Heat Transfer to Constant and Variable Property Fluids in Turbulent Pipe Flow," Dept. of Chem Engr., University of Washington, Seattle, Washington 98195, July 1974.

29. Carpenter, F.G., Colburn, A.P., Schoenborn, E.M., and Wurster, A., “Heat Transfer and Friction of Water in an Annular Space,” Transactions of the AIChE, Vol. 42, pp. 165-187, 1947.
30. Petukhov, B.S. “Heat Transfer and Friction in Turbulent Pipe Flow with Variable Physical Properties,” Advances in Heat Transfer, Vol. 6, pp. 503-564, 1970.
31. Bergles, A. E. and Rohsenow, W. M., "The Determination of Forced Convection Surface-Boiling Heat Transfer," J. Heat Trans., Vol. 86, pp. 365-372, August 1964.
32. McAdams, W.H., Kennel, W.E., Minden, C.S., Rudolf, C., Picornell, P.M., and Dew, J.E., “Heat Transfer at High Rates to Water with Surface Boiling,” Massachusetts Institute of Technology, Cambridge, Massachusetts, 1945.
33. Kutateladze, S. S., "Boiling Heat Transfer," Int. 1. Heat Mass Trans., Vol. 4, pp. 31-45, 1961.
34. Forster, K. and Greif, R. “Heat Transfer to a Boiling Liquid-Mechanism and Correlations,” Journal of Heat Transfer, Ser. C, Vol. 81, No. 1, pp. 43-53, February 1959.
35. Gambill, W. R., "Generalized Prediction of Burnout Heat Flux for Flowing, Subcooled, Wetting Liquids," Chem. Engng Progr. Symposium Series, Vol. 41, No. 59, pp. 71-87, 1963.
36. Feldman, E.E., “Implementation of the Flow Instability Model for the University fo Missouri Reactor (MURR) That is Based on the Bernath Critical Heat Flux Correlation,” ANL/RERTR/TM-11-28, Attachment 2 Argonne National Laboratory, July 2011.
37. Bernath, L., "A Theory of Local-Boiling Burnout and Its Application to Existing Data," Chem. Engng Progr. Symposium Series, Vol. 56, No. 30, , pp.95-116, 1960.
38. Levy, S., "Prediction of the Critical Heat Flux in Forced Convection Flow," GEAP-3961, General Electric Rpt., San Jose, California, June 1962.

39. Labuntsov, D.A., “Critical Thermal Loads in Forced Motion of Water Which is Heated to a Temperature Below the Saturation Temperature,” Soviet Atomic Energy, Vol. 10, No. 5, pp. 516-518, March 1962.
40. Vandervort, C. L., Bergles, A. E., and Jensen, M. K. “The Ultimate Limits of Forced Convective Subcooled Boiling Heat Transfer.” Rensselaer Polytechnic Institute Heat Transfer Laboratory Report HTL-9, May 1992.
41. Ornatskii, A.P., Vinyarskii, L.S., “Heat Transfer Crisis in a Forced Flow of Underheated Water in Small-Bore Tubes,” High Temperature, Vol. 3, pp. 400-406, 1965.
42. Beitel, G.R., Savage, K.P., Catalano, D.R., Hiers, R.S. III, “Combustor Imaging Probe for Gas Turbine Engines,” AIAA 2007-5717, 43rd Joint Propulsion Conference & Exhibit, Cincinnati, Ohio, July 8-11, 2007.
43. Beitel, G.R., Catalano, D.R., and Edwards, R., “Electroformed Diagnostic Probes for High-Temperature Gas Flows,” AIAA 2004-5717, 24th Aerodynamic Measurement Technology and Ground Testing Conference, Portland, Oregon, June 28 – July 1, 2004.
44. Beitel, G.R., “A Review of Boiling Heat Transfer Processes at High Heat Flux,” AEDC-TMR-92-V1, Arnold Engineering Development Center, Arnold Air Force Base, TN, April 1991.
45. Bergles, A. E. “Future Directions of Research in Multi-Phase Flow and Heat Transfer.” Multiphase Transport-Fundamentals, Reactor Safety, Applications, edited by T. N. Veziroglu, Vol. 1, 1980, pp. 3-18.
46. Rohsenow, W. M. “Boiling,” Annual Review of Fluid Mechanics – Vol. 3, pp. 211-236, 1971.
47. Rohsenow, W. M., "Heat Transfer with Evaporation," Heat Transfer... A Symposium, Summer 1952, Chapter 4, pp. 101-149, Eng. Res.Inst., Univ. of Mich., Ann Arbor, MI 1953.
48. Yuan, B., Zhang, Y., and Jinjia, W. “Theoretical CHF predicted model for subcooled flow boiling,” Journal of Heat and Mass Transfer, Vol 55, pp. 2437-2444, September 2019.

49. Rohsenow W. M. “Heat Transfer with Boiling,” Chapter 8, Developments in Heat Transfer. W. M. Rohsenow, Editor, MIT Press, 1964.
50. Jens, W.H. and Lottes, P.A. “Analysis of Heat Transfer, Burnout, Pressure Drop and Density Data for High-Pressure Water,” ANL-4627, Argonne National Laboratory, Naval Reactor Division, Chicago, Illinois, May 1951.
51. Sieicher, C. A. and Rouse, M. W., "A Convenient Correlation for Heat Transfer to Constant and Variable Property Fluids in Turbulent Pipe Flow," Int. 1. Heat Mass Trans., Vol. 18, pp. 677-683, 1975.
52. White, F. M., “Fluid Mechanics,” McGraw-Hill, New York, New York, 1979.
53. Jain, P. K., Nourmohammadi, K., and Roy, R. P., "A Study of Forced Convection Subcooled Boiling in Heated Annular Channels," Nucl. Eng. Design, Vol. 60, No.3, p. 401-411, 1980.
54. Ishii, M. and Mishima, K., "Two-Fluid Model and Hydrodynamic Constitutive Relations," Nucl. Eng. Des., Vol. 82, pp. 107-126, 1984.
55. Forster, H. K. and Zuber, N., "Growth of a Vapor Bubble in a Superheated Liquid," J. ofApplied Physics, Vol. 25, No.4, pp. 474-478, April 1954.
56. Shah, M. M., "Generalized Prediction of Heat Transfer during Subcooled Boiling in Annuli," Heat Trans. Engng, Vol. 4, No.1, pp. 24-31, 1983.
57. Bjorge, R. W., Hall, G. R., and Rohsenow, W. M., "Correlation of Forced Convection Boiling Heat Transfer Data," Int. J. Heat Mass Trans., Vol. 25, No. 6, pp. 753-757, 1982.
58. Bergel'son, B. R., " Burnout under Conditions of Subcooled Boiling and Forced Convection," Thermal Engng, Vol. 27, No.1, pp. 48-50, 1980.
59. Moeller, T.M., Rhodes, R., Beitel, G.R., and May, M.M., “Prediction and Experimental Measurement of Total Temperature in an Afterburning Turbojet Exhaust,” AIAA 2012-0811, 50th Aerospace Sciences Meeting, Nashville, Tennessee, January 09-12, 2012.
60. Wang, E.N., “Advanced Nanostructures for Two-Phase Fluid and Thermal Transport,” AFOSR Grant FA9550-11-1-0059, MIT, Cambridge, MA, October 8, 2014

61. Rousar, D.C. and Van Huff, N.E. “Heat-Transfer Characteristics of 98% H_2O_2 at High Pressure and High Velocity,” AFRPL-TR-66-263, August 1966.
62. Kharangate, C.R., O’Neill, L.E., and Mudawar, I. “Effects of two-phase inlet quality, mass velocity, flow orientation, and heating perimeter on flow boiling in a rectangular channel: Part 2 – CHF experimental results and model,” International Journal of Heat and Mass Transfer, Vol 103, pp. 1280-1296, December 2016.
63. Rousar, D.C., Van Huff, N.E., Roger, A.E. and Fink, A. “Heat Transfer Study of MHF-5 and MMH,” AFRPL-TR-67-208, Declassified on 05 Feb 1986, August 1967.
64. Ornatskii, A.P. and Vinyarskii, “Heat Transfer Crisis in a Forced Flow of Underheated Water in Small-Bore Tubes,”
65. Levy, S., "Generalized Correlation of Boiling Heat Transfer," J. of Heat Transfer, Vol. 81, pp. 37-42, February 1959.
66. Beitel, G.R., Moeller, T.M., May, M.M., “Cooling of Miniature Flow-Field Probes for Combustion Measurements,” AIAA 2011-3485, 42nd Thermophysics Conference, Honolulu, Hawaii, June 27-30, 2011.

VITA

Joshua L. Osborne was born in Huntington, West Virginia in May 1985 to Mr. H. Lee Osborne and Mrs. Brenda G. Long. In 2004, while a freshman in college, Joshua enlisted in the United States Air National Guard out of Martinsburg, West Virginia and received an honorable discharge as a staff sergeant in 2010 after six years of service. In 2008, Joshua graduated from West Virginia University in Morgantown, West Virginia with a Bachelor of Science in Mechanical Engineering. After graduating from West Virginia University, Joshua began his engineering career in 2008 working for B/E Aerospace as a manufacturing engineer. In 2010, Joshua came to work for the United States Air Force at Arnold Engineering Development Complex where he has performed duties as an aeropropulsion analysis engineer, test engineer, test manager, technology project manager, senior engineer for test capabilities integration, and most recently just assumed the position of Section Chief for Future Capabilities. Joshua enrolled in the graduate program at the University of Tennessee Space Institute in the fall of 2011, and plans to further pursue his education towards an Engineering doctoral degree.